Thermodynamic performance analysis and optimization of a power and hydrogen generation system based on geothermal flash, dual-pressure organic Rankine cycle using zeotropic mixtures, and PEM electrolyzer

Seyed Saman Ashraf Talesh (s.s.ashraf.t@gmail.com)
University of Mohaghegh Ardabili

Research

Keywords: Flash-binary geothermal power plant, DORC, PEM electrolyzer, Energy and exergy analysis, Optimization

Posted Date: October 7th, 2020

DOI: https://doi.org/10.21203/rs.3.rs-87960/v1

Thermodynamic performance analysis and optimization of a power and hydrogen generation system based on geothermal flash, dual-pressure organic Rankine cycle using zeotropic mixtures, and PEM electrolyzer

Seyed Saman Ashraf Talesh [a,*]

[a] *Department of Mechanical Engineering, University of Mohaghegh Ardabili, Ardabil, Iran*

Abstract

In this study, a thermodynamic model and optimization of a flash-binary geothermal system are proposed for power and hydrogen production. The binary cycles contain a dual-pressure ORC cycle and proton exchange membrane electrolyzer for power and hydrogen production. The combination of dual-pressure organic Rankine cycle with zeotropic mixtures enhances the performance of the system considerably, and selection of the best kind of zeotropic mixture as the working fluids of the DORC unit is one of the important methods to improve the performance of the suggested system. Also, the Genetic algorithm is employed to optimize the net output power of the system, in which the results of optimization show that the best performance belongs to Pentane (0.467)/Butane (0.533) with first and second-law efficiencies of 16.66%, 58.03%, respectively, and hydrogen production of $0.3683\ kg/hr$. Besides, for the base case simulation, the energy and exergy efficiencies of the whole system are reported by about 16.66% and 58.03%, respectively, also for this condition, the derived power from the proposed model and overall exergy destruction is calculated approximately $132.41\ kW$, and $90.08\ kW$, respectively and geothermal heat source generates $0.306\ kg/hr$ hydrogen by the proton exchange membrane electrolyzer.

[*] *Corresponding Author, E-mail address: s.s.ashraf.t@gmail.com*

Keywords: Flash-binary geothermal power plant; DORC; PEM electrolyzer; Energy and exergy analysis; Optimization

Nomenclature

Symbols

C	thermal conductivity ($W.m^{-1}.K^{-1}$)
D	equilibrium phase vapor density
$\dot{E}$	exergy rate (kW)
$\dot{E}_D$	exergy destruction rate (kW)
h	specific enthalpy ($kJ.kg^{-1}$)
$\dot{m}$	mass flow rate ($kg.s^{-1}$)
MM	molar mass
P	pressure (MPa)
$\dot{Q}$	heat flow rate (kW)
s	specific entropy ($KJ.kg^{-1}.K^{-1}$)
T	temperature (K)
v	dynamic viscosity ($Pa.s$)
$\dot{W}$	power (kW)

Greek Symbols

η	Efficiency (%)

Abbreviations

DORC	Dual-pressure Organic Rankine Cycle
GA	Genetic Algorithm
OTEC	Ocean Thermal Energy Conversion
ORC	Organic Rankine Cycle
PEM	Proton Exchange Membrane

Subscripts and superscripts

q	Heat transfer
sys	System
th	termal
tot	total
1, 2, …	cycle locations
0	Dead state

ε	effectiveness
ω	mass fraction

1. Introduction

In the last years, due to the climate changes and ozone layer depletion, energy policies in various countries are implemented. Because of the mentioned environmental issues for the energy production process by fossil fuels and reduce this dependency, renewable energy sources are employed as a cost-effective alternative [1]. Recently, the use of clean energy resources like solar, geothermal, and wind are considerably planned by governments. In addition, the research and development of novel technologies with high efficiency are designed by researchers [2]. The Organic Rankine Cycle (ORC) is known as one of the popular systems to generate electricity with high capability, in which the working fluid is ranged from low to medium-enthalpy [3]. The geothermal energy with the properties of sustainable and low temperature has a significant role to be applied for the ORC systems [4]. among all of the energy extraction systems, binary and flash-binary units illustrate high performance in compared with the others. Yari [5] presents a comprehensive comparison for the various kinds of geothermal systems, the results of this paper shows that the flash-binary plant has the best performance with the efficiency of the 11.81 % when the mass flow rate and the temperature of the heat source of geothermal energy are 1 kg/s, and 230 ℃, respectively. Jalilinasrabady and Itoi [6] investigated about the three different systems, including binary, single, and double flash units, from their works, the best performance is obtained for the binary ORC system. From the thermodynamic and thermoeconomic aspects, various geothermal cycles (binary, single, and double flash units, and kalina cycle) are compared

and analyzed [7]. The results show that the optimum electricity production is founded with respect to the pressure of the flash chamber and turbine input pressure for double-flash and integrated flash-binary cycles. Shokati et al. [8] investigated about the single and binary-flash cycle comparison under thermoeconomic vantage point. Based on this work, the best first and second thermodynamic law efficiencies are founded for the single-flash Organic Rankine Cycle. A new multigeneration system with the aim of power and hydrogen production based on flash-binary geothermal resources is proposed by Yilmaz et al. [9]. The obtained data show that the system produces $0.04981 kg/s$ hydrogen when the geothermal resource temperature and mass flow rate are 200 ℃, and $100\ kg/s$, respectively. Choosing a desirable working fluid for a flash-binary combined unit was performed by Ref. [10]. It's claimed that an optimum separator pressure can be founded for every working fluids and related to these optimum values, the efficiency and exergy destruction of the cycle can be optimized. Besides, some working fluids for the special range of geothermal temperatures illustrate proper performance. Zhao and Wang [11] assessed the ORC system as a flash-binary system, and the different design parameters are evaluated under exeroeconomic performance of the proposed cycle. The results show that at the best performance from exeroeconomic analysis, the highest energy and exergy efficiencies may not result and vice-versa. The analysis of exergy destruction at the ORC systems is introduced as one of the main challenges, especially at the evaporative, due to the inconformity between hot and cold fluid [12]. The destruction of the exergy of evaporative can be decreased by some approaches such as trilateral, flash binary, and two-stage units and also zeotropic mixtures. Researchers in recent years investigated the zeotropic mixture concept due to its extremely interesting performance. The zeotropic mixtures have non-isothermal phase transitions at constant pressure. The isothermal condensing and evaporating is the largest deficiency of a pure

fluid into the ORC system so that the zeotropic mixture is known by non-isothermal phase transition at constant pressure. These fluids matched the heat source and sink profiles, decreased the irreversibility, and enhanced the performance of the cycle. The utilization of the zeotropic mixture in Organic Rankine Cycle is investigated by the Chys et al. [13]. According to their results, by applying the zeotropic combination in comparison with the pure fluid. The energy efficiency of the system at the input temperature of 150 ℃ and 250 ℃ is enhanced about 16% and 6%, respectively The power generated by the ORC system utilizing the zeotropic mixture and low-grade heat source was done by Heberle et al. [14], in which the mixtures of R227ea-R245fa and Isobutane-Isopentane are used as working fluid of the cycle. Referring to this work, the efficiency related to second-low compared with pure fluid was improved about 15 %, when the energy source temperature is lower than 120 ℃. At another work, the effect of the zeotropic combination on the exergy efficiency of the ORC system driven by geothermal energy resource is analyzed by the Lecompte et al. [15]. The obtained data show that the second law efficiency can be improved from 7.1 % to 14.2 % in comparison with pure fluid. The effectiveness of the zeotropic mixture on the net power output of the proposed supercritical ORC system driven by the low-grade resource is evaluated in Ref. [16]. The results of their work presented that the use of zeotropic mixture leads to enhance the energy efficiency of approximately15% compared to the pure R-134a at a similar operation condition. Zhang et al. [17] designed a regenerative ORC system based on operating fluids of pure R245fa and (with $0.7 - 0.3$ mass fraction) using the waste heat of diesel engines. According to their results, using the zeotropic mixture result in better performance of the hybrid plant, so that the power generation of the system is increased by about 10.54 %, and the fuel consumption is reduced by about 9.55%. the impact of the different zeotropic mixture on the various construction of ORC systems that are driven by geothermal

energy source is assessed by Sadeghi et al. [18]. Concerning their work, in contrast to the pure fluid, the values of power generation are enhanced from 24.79% to 27.76% by the zeotropic mixture.

A number of the works focused on the system construction to improve the performance of cycles. Different constructions for organic Rankine cycles are investigated by Ho et al. [19]. According to their obtained data to improve the power generation, by splitting the expansion process into two steps and combining the liquid stream from flash evaporation in a secondary expansion stage, utilization efficiency gains of 10% above the optimized basic Organic Rankine Cycle (ORC) are achievable. Besides, a dual-pressure binary system is studied by the Kanoglu [20] under the exergy viewpoint, and the energy efficiency of proposed systems was improved to about 5.8% and 8.9%. Another dual-pressure evaporation organic Rankine cycle is presented in Ref. [21] that is powered by the heat source temperature between $100-200°C$. Nine pure fluid was chosen as the working fluids of the proposed cycle, and the results show that with the inlet temperature decreases, the net output power generation is maximized. The optimum values of net power output power are ranged between $21.4-26.7\%$ for nine selected working fluids.

Different energy resources like geothermal, solar, biomass, and natural gas can be implemented to produce hydrogen [22]. Besides, different ways can be employed for hydrogen production under the electrolysis method, such as proton exchange membrane (PEM), and solid oxide fuel cell and alkaline. The hydrogen production as an energy carrier has high importance when renewable energy resources are applied due to its influence on the pollutions decreasing. Amongst all of the approaches, the proton exchange membrane electrolyzer illustrates a high potential where green energy resources are utilized. Ni et al. [23] investigate exergy and energy efficiency for the PEM electrolysis device. From their results, exothermic state as the heat-

producing was obtained for the PEM electrolysis and it is revealed that the operational temperature of the PEM electrolysis, thickness of electrolyzer, and current density effect on the energy performance of the system. Another improved PEM device, considering modular mathematical models of electrolyte, the voltage of cell, negative and positive electrolyte, is employed in Ref. [24]. To improve the selected parameters, an enhanced model of a PEM electrolyzer cell is presented, based on linked modular mathematical models of the anode, cathode, membrane and cell voltage. A great current density is exchanged by anode in an enhanced PEM electrolyzer, which results in a significant improvement of performance. A solar-enhanced proton exchange membrane using Ocean Thermal Energy Conversion (OTEC) as the green energy resource for hydrogen production is evaluated in Ref. [25]. An organic Rankine cycle is applied to support the energy demand of the PEM device. According to the obtained data, efficiency of energy and exergy of the suggested model were increased by about 3.6%, and 22.7%, respectively. Besides, the produced hydrogen and exergy efficiency of PEM were assessed about $1.2 kg/hr$ and 56.5%, respectively.

Up to our knowledge, the previous works are mostly focused on utilizing various pure fluids and mixtures that are designed for simple systems with geothermal resources and also different ORC system constructions. A few numbers of works are implemented with respect to zeotropic combinations in the flash cycle based DORC unit. Besides, to the best of authors' knowledge and through the literature survey, integration of geothermal energy source with a dual-pressure evaporation ORC system and PEM electrolyzer based on using zeotropic mixtures has not been investigated yet. So that, a new integration of zeotropic mixtures (Pentane/Butane, pentane/Cis-2-butene, and Pentane/Trans-2-butene) based-ORC unit with Proton Exchange Membrane

electrolyzer is performed for power and hydrogen production by for supplying a proportion of vehicle filling station's fuel.

Main objectives of the present paper are summarized as:

- A new configuration for hydrogen and power production is implemented based on a geothermal flash cycle, dual-pressure ORC system with zeotropic mixtures as working fluids, and PEM electrolyzer.
- A thermodynamic analysis and optimization process are done for the flash-binary system, and the key parameters of the suggested system are computed.
- Zeotropic mixtures with different combinations are used for reaching the best performance of the proposed system.
- The generated electricity power, amount of hydrogen production, energy/exergy outputs, and their efficiency and also optimization of the proposed system are analyzed.

1. Methodology

1.1. Description of system

The schematic view of the proposed system is demonstrated in Fig.1. According to this figure, the system is divided into two systems: 1- the flash cycle that is employed for the geothermal energy extraction, 2- dual pressure-evaporation ORC system, and PEM electrolyzer that is known as the binary units for power and hydrogen production. The geothermal energy is extracted by the flash system, in which to reach a low-pressure flow, the extracted fluid from geothermal is isenthalpically expanded by the expansion valve. The flash chamber separates the low-pressure and two-phase flow into two saturated liquid and steam flows. The saturated steam flow goes into the turbine, which is expanded for power production, and the exit stream from the turbine enters the condenser and cools down to the lower temperatures. The saturated liquid

leaves the flash chamber and is delivered to the evaporators (1) and (2) and heat exchanger (1) to adjust the demanded energy of the flash cycle. The required electricity and thermal energy to operate the PEM electrolyzer is supported by the ORC turbine and HX (2), respectively. Finally, the exit fluid of the HX (2) combined with the leaving fluid of condenser (2) and is fed to the reinjection well.

In addition, for the dual-pressure organic Rankine cycle, the pressure of the zeotropic fluid is increased by the low-pressure pump (1) and is heated up under leaving the HX (1). Then the working fluid is separated in the splitter, one section of the divided fluid is converted to the saturated flow by the evaporator (2), and another section of the flow is delivered to the pump (2) and then is fed to the Eva (1). So, the zeotropic fluid is saturated when gains enough thermal energy from the evaporator (1) and was pressurized by the pump (2). The working fluid after leaving the evaporator (1) with high-pressure goes into the turbine (ORC HP Turbine) and is expanded for power generation, where losses its pressure. The exiting fluid from the HP turbine is mixed with the exhaust saturated steam from the low-pressure evaporator (Eva (2)) and is delivered to the low-pressure turbine for extra power generation. Ultimately, at the flash-binary cycle, including zeotropic mixtures ORC subsystem, the condenser (Cond (1)) gains the heat of the low-pressure output flow, and the fluid is converted to the saturated liquid. Based on the $T-s$ diagram of the dual-pressure organic Rankine cycle, the temperature glides due to the zeotropic mixtures at the two-phase sections are clearly shown in Fig.2.

1.2.Working fluid determining

The pure water is assumed as the geothermal fluid of the flash cycle, and the analysis of this section of the system is done based on the pure water features. Besides, the evaluations of the DORC unit are performed according to the various organic fluids which are introduced as the

zeotropic mixtures. The choosing of the fluids type to access the best performance of the proposed system is at the center of attention. So, for the proper selection, the following indicators and characteristics should be regarded:

- Medium critical temperature and pressure.
- High value for the thermal conductivity and low viscosity that led to high heat transfer and low frictions loss in heat exchanger.
- The safety and chemical stability, including flammability and toxicity, must be regarded.
- For the special amount of energy received for the system, the optimum values for first and second low efficiency and also net output power should be assessed.
- The slope of the vapor curve always is positive, and for the negative values, at the turbine blades, the droplet generation can be seen.
- Environmentally friendly based on ozone-depleting potential (ODP) and Global Warming Potential (GWP).

Based on the above-mentioned specifications, the determining of a suitable working fluid with all assumptions simultaneously can be caused by several limitations. The zeotropic fluids to overcome these problems instead of pure fluids are employed. For better certification, zeotropic mixtures can be used as proper candidates for organic Rankine cycle working fluids because of its good matching between temperatures of the heat source (based on the temperature glide in processes of heat exchangers (evaporation, condensation, and regeneration)) and working fluids. In this paper, Pentane/Butane, pentane/Cis-2-butene, and Pentane/Trans-2-butene as (dry/dry) zeotropic mixtures are assessed to calculate the novel proposed ORC performance. The thermodynamic properties of the selected zeotropic mixtures are tabulated in Table 1.

2. Mathematical modeling

In this paper, energy and exergy equations are used for the evaluation of proposed system performance. Assumed considerations for thermodynamic modeling of a new combined system to simplify the MATLAB computation are as follow:

- The steady-state conditions are assumed for all of the constitutes in the cycles [26, 27]
- The heat and friction losses in all of the heat exchangers are ignored [26, 27].
- The kinetic and potential energy of water as the heat source is not be considered.
- The heat transfer variables are assumed as the entirely developed flow.
- The condition of zero state (dead-state condition) is set to $T = 293.15K$ and $P = 1atm$ [28].

Besides the above-mentioned considerations, several other cases and conditions are required to assess the suggested system are given Table 2, and also, the simulation is done by MATLAB software so that the REFPROP toolbox is applied to call the thermodynamic features of the operational fluid [28].

2.1.Energy and exergy analysis

The related equations for the mass, energy, and exergy balance are represented as follows [29]:

$$\sum \dot{m}_{in} = \sum \dot{m}_{out} \tag{1}$$

$$\dot{Q} - \dot{W} = \sum \dot{m}_{out} h_{out} - \sum \dot{m}_{in} h_{in} \tag{2}$$

$$\dot{E}_Q - \dot{W} = \sum \dot{m}_{out} e_{out} - \sum \dot{m}_{in} e_{in} + \dot{E}_D \tag{3}$$

In which, $\dot{m}$ is the mass flow rate; the inlet thermal energy and net output power is respectively denoted by $\dot{Q}$ and $\dot{W}$; h is known as the specific enthalpy, and $\dot{E}_D$ illustrate the destruction rate of

exergy. In addition, the exergy rate from heat transfer($\dot{E}_Q$), and specific exergy flow is presented by the Eqs. 4 and 5.

$$\dot{E}_Q = \sum \dot{Q} \left(1 - \frac{T_0}{T}\right) \quad (4)$$

$$e = h - h_0 - T_0(s - s_0) \quad (5)$$

The relations of all components based on mass, energy, and exergy analysis are represented in Table 3 and Table 4. The parameters of exergy analysis, including fuel exergy, product exergy, exergy destruction, and exergy efficiency for every component is given in Table 4.

2.2.PEM electrolyzer

The required power for the proton exchange membrane electrolyzer to drive electrochemical reactions is produced by the DORC cycle, where the liquid water with ambient condition delivers to the heat exchanger (2) to increase its temperature up to the PEM electrolyzer temperature, and the preheated water is heated up by the heater. Ultimately, the hot water enters the PEM electrolyzer to produce hydrogen. Generated hydrogen after leaving the cathode cools down to environmental temperature; on the other side, the oxygen is separated from water, and the extra unreacted water is mixed again with the supply line of hot water for hydrogen production. The demanded energy of PEM electrolyzer is given as follows [30, 31]:

$$\Delta H = \Delta G + T\Delta S \quad (6)$$

Here, ΔG is the demanded electrical energy (Gibb's free energy), and $T\Delta S$ is the required thermal energy [$\frac{J}{mol}.H_2$].

The electrolyzer potential with assuming that the $J < 10{,}000\frac{A}{m^2}$ [32], and ignoring the concentrating losses, can be calculated as:

$$V = V_0 + V_{act,a} + V_{act,c} + V_{ohm} \quad (7)$$

Where, V_0 depicts the reversible potential which can be driven by the Nernst relation, besides, $V_{act,a}, V_{act,c}$ are the activation over-potential of the cathode and anode, respectively and V_{ohm} present the ohmic over-potential of the electrolyte. The reversible potential and ohmic voltage loss are computed by:

$$V_0 = 1.229 - 8.5E - 4 * [T_{PEM} - 298] \quad (8)$$

$$V_{ohm} = J * R_{PEM} \quad (9)$$

R_{PEM} and J are the overall ohmic resistance current density,that computed by [32], [33]:

$$R_{PEM} = \int_0^d \frac{dx}{\sigma_{PEM}[\lambda(x)]} \quad (10)$$

Herein, $\sigma(x)$ is the local ionic conductivity which is given by:

$$\sigma_{PEM}[\lambda(x)] = [0.5139 * \lambda(x) - 0.326] * e^{1268*\left[\frac{1}{303}-\frac{1}{T}\right]} \quad (11)$$

In which, $\lambda(x)$ depicts the water content at location x (membrane depth from the cathode membrane) and are expressed by:

$$\lambda(x) = \frac{\lambda_a - \lambda_c}{L} * x + \lambda_c \quad (12)$$

Whereas, L denotes the membrane thickness; λ_a and λ_c indicate the water contents at the anode-membrane and cathode-membrane interface, respectively.

As well, $V_{act,a}$ and $V_{act,c}$ are the electrodes' activity metrics and are presented in the following form [32]:

$$\begin{cases} V_{act,a} = \frac{RT}{F} * \sinh^{-1}\left[\frac{J}{2J_{0,a}}\right] \\ V_{act,c} = \frac{RT}{F} * \sinh^{-1}\left[\frac{J}{2J_{0,c}}\right] \end{cases} \quad (13)$$

In this equation, j_0 is the exchange and can be calculated by [32]:

$$\begin{cases} J_{0,a} = J_a^{ref} * e^{\left[-\frac{E_{act,a}}{RT}\right]} \\ J_{0,c} = J_c^{ref} * e^{\left[-\frac{E_{act,c}}{RT}\right]} \end{cases} \quad (14)$$

In this relation, J^{ref} presents the pre-exponential factor; E_{act} denotes the activation energy.

Also, in the positive and negative electrodes, the molar flow rates of the produced hydrogen and oxygen are addressed by:

$$\dot{N}_{H_2} = \frac{J}{2F} \quad (15)$$

$$\dot{N}_{O_2} = \frac{J}{4F} \quad (16)$$

Whereas, J indicates current density and F is Faraday constant. More details are presented in [34].

2.3.Performance criteria

The energy and exergy performances of the thermal plants can be described as:

$$energy\ performance = \frac{energy\ of\ products}{entire\ input\ energy} \quad (17)$$

$$exergy\ performance = \frac{exergy\ of\ products}{entire\ intput\ exergy} \quad (18)$$

The efficiencies of the energy and exergy for the proposed system can be expressed as follows:

$$\eta_{I_{tot}} = \frac{\dot{W}_{tot} + \dot{m}_{H_2}.LHV_{H_2}}{\dot{m}_1(h_1 - h_{27})} \quad (19)$$

$$\eta_{II_{tot}} = \frac{\dot{W}_{tot} + \dot{E}_{25}}{\dot{E}_{in}} \quad (20)$$

Whereas;

$$\dot{W}_{tot} = \dot{W}_{ST} + \dot{W}_{ORC} - \dot{W}_{PEM} \quad (21)$$

$$\dot{W}_{ORC} = \dot{W}_{OT} - \dot{W}_P \quad (22)$$

2.4.Optimization

To reach the optimal solution in the problems, the Genetic Algorithm (GA) can be implemented as a heuristic optimization method. Genetic algorithm is a stochastic optimization technique, which is inspired under the natural selection laws and genetics. John Holland [35-38] initially enhanced the concept of this optimizer based on the Darwin's theory of evaluation, where the fitter individuals are likely to survive in a competing environment. GA algorithm has no need for functional derivative information to explore the solution set because this method is derivative-free in a sense, and the given objective function is minimized. As the advantages of this approach, GA decreases the burden of calculation and time of search as well as solves the complex objective functions. In this algorithm, each solution is assumed as a particle (chromosome), and the population includes several chromosomes, which is created by the random method as a low computational method. Every particle leads to a fitness value. For the stop state of the iteration, a selected number is employed. Between the particles, the determining pairs of particles with high fitness is in priority. In addition, a crossover approach is utilized for every pair to select the particles where the new particles are created. For the selection of some

other particles is performed for the application of the mutation operator to generate new particles. Fitness amounts most be evaluated for all of the iterations of particles, and the best particle is founded. At the end of the iteration, the optimal particle will be determined [39].

In this work, the optimal values of the objective function are obtained based on the genetic algorithm. Maximizing the value of entire output power ($\dot{W}_{tot}$) is the main aim of this work. The objective function reduces to maximize just the $\dot{W}_{ORC}$. The $\dot{W}_{ST}$ has no changing with the variation of the optimization variables (according to the Eq. (21)). This is worthy to state that, the optimization of the top and low temperature of DORC unit (T_{top}, T_{low}) is the main objective. The considered objective is mathematically expressed by:

$$\dot{W}_{ORC} = f\left(m_f, T_{top}, T_{low}\right) \tag{23}$$

Whereas, m_f indicates the mass fraction; besides, the below limitations should be implemented:

$$\begin{cases} \Delta T_{PPEv} \geq 15K \\ \Delta T_{PPC2} \geq 10K \\ \varepsilon \geq 50\% \\ \dot{E}_D > 0 \end{cases} \tag{24}$$

And;

$$\begin{cases} 0 \leq m_f \leq 1 \\ T_{low} < T_{top} < T_{cr} \\ T_0 < T_{low} < T_{top} \end{cases} \tag{25}$$

For the above-mentioned limitations, $\Delta T_{PPEv}, \Delta T_{PPC2}$present the pinch point temperature for the evaporator and condenser, respectively. ε depicts the heat exchangers efficiencies at the phase-

change condition, which is assumed bigger than 50% [40]. The flowchart related to the GA optimization method is illustrated in Fig. 3.

3. Results and discussion

3.1.Model validation

In order to model the new combined model for the power and hydrogen production, a simulation code applied REFPROP toolbox in MATLAB software is developed. According to obtained data from the simulation, the results are validated with the three previous work [41-43]. The validations are done for the dual-pressure ORC, PEM electrolyzer unit, and geothermal flash cycle. Fig. 4 illustrates a comparison between the obtained data of DORC unit of present work and the results that are reported by Li et al. [42]. According to this figure, the variation of the energy efficiency of the DORC in contrast to the different mass fractions for the Isobutane/Isopentane mixture is plotted. Also, the changes in the cell voltage due to the variation of the cell density to indicate the validation of the PEM electrolyzer unit is shown by Fig. 5. Eventually, to certificate the performance proposed system, the behavior of the suggested model steam turbine is compared with the results that are reported by Yilmaz et al. [41] and are presented in Fig. 6. Referring to the Figs. 4, 5, and 6, there are good agreements between the obtained results in the present model and those reported in the literature.

3.2.Parametric analysis of system performance

3.2.1. Mass fraction impact on the performance of the system

In this section, the temperatures of the first evaporator and condenser are considered about $428.81\,K$ and $313\,K$. Also, the pinch point temperature differences of these components are assumed to be $15\,K$ ad $10\,K$, respectively. For the different mass fraction, under various

zeotropic mixtures, the variation of mass flow rates is shown in Fig.7 (a). According to the results of this figure, with increasing of the mass fraction, the mass flow rate until specific range decreases and then continues with the rising trend so that the minimum value obtained for Pentane/Cis-2-butene fluid. Figs 7 (b-e) indicates the behavior of the net output power as well as the energy efficiency of the proposed system in contrast to the mass fraction changes. What stands from these figures is that firstly the power production rate and first-law efficiency increase with increment of the mass fraction of zeotropic mixtures, and after that, the intended fluids decrease. Due to this trend, an optimum value can be seen for each zeotropic mixtures; as presented in Fig. 7 (b) and (c), the best values related to the produced power through the DORC unit and net output power of system belong to the Pentane/Butane; this is due to this fact that the change of produced electricity not only relates to mass fractions but also depends to net specific power.

Besides, the total energy efficiency and thermal efficiency of dual-pressure evaporation system is depicted in Fig. (7) d and (e). the above-mentioned mathematical equations justify that the firs-law efficiency of the whole system depends on the temperature and mass flow rate of geothermal fluid, power utilized by the PEM electrolyzer and also net output power. It is good to mention that the geothermal temperature and mass flow rate are constant; the produced power from the flash-binary subsystem affects the energy efficiency of the entire system. Therefore, the best performances of the suggested system are obtainable at the mass fraction range of [0.4-0.6], and the maximum energy efficiency of the DORC system and the whole system is reported for Pentane/Butane and Pentane/Cis-2-Butene about 11.332 % and 16.74 %, respectively. Also, the variation of the produced hydrogen due to the different values of mass fraction for three assumed working fluids are represented in Fig. 7 (f), referring to this figure, the Pentane/Butane as the

zeotropic mixture has the highest amount of generated hydrogen, this optimum production is due to the power used by the PEM electrolyzer.

Fig.8 illustrates the exergy destruction rate in every constitute of the proposed system for the different mass fraction of considered zeotropic mixtures, including Pentane/Butane, Pentane/Trans-2-Butane and Pentane/Cis-2-Butene. As shown in Fig. 8 (a), the rate of exergy destruction of Eva (1) and Eva (2) firstly decreases and then increases, and for heat exchanger (1), the exergy destruction firstly drops, then rises. Minimum exergy destruction for Eva (1) and Eva (2) is reported about $8.83\ kW$ and $4.07\ kW$ for mixtures of Pentane/Trans-2-Butene and Pentane/Butane, respectively. Besides, the rate of exergy destruction of Cond (1), Pumps and Turbines is illustrated in Fig. 8 (b), as can be seen in Fig. 8 (b), the turbines exergy destruction grow up until the mass fraction of 0.2, and after that exergy destructions reduce. Maximum exergy destruction is approximately $6.97\ kW$ for the Pentane/Butane mixture. In addition, the condenser (1) has similar behavior to the evaporator, in which the minimum exergy destruction is assessed for the Pentane/Trans-2-Butene working fluid about $9.4\ kW$, for the mass fraction of 0.5, for pumps, the exergy destructions of assumed working fluids are almost steady up with a decreasing slope in all of the mass fraction intervals.

The overall exergy destruction of the system can be achieved by summation of the exergy destruction of each component. The exergy destruction related to the dual-pressure organic Rankine cycle unit is indicated in Fig. 9 (a), and the total exergy destruction is plotted in Fig.9 (b). It can be pointed out clearly that these two figures have the same trend in the different mass fractions because the DORC flash-binary system is dominated over the geothermal flash cycle. The second-law efficiency of the dual-pressure organic Rankine cycle system and the whole system is respectively shown in Fig. 9 (c) and Fig. 9 (d). The exergy efficiency of system

depends on the net output work and exergy of geothermal fluids. As mentioned above, the condition of geothermal fluid is constant, so the behavior of net output power and second-law efficiency of the entire system is similar. The lowest exergy efficiency of the system is founded at the highest exergy destruction, in which the mixtures of Pentane/Trans-2-Butene in a mass fraction of 0.5 has the highest exergy efficiency.

3.2.2. Operating parameters impact on system performance

In this study, energy and exergy investigation has been carried out based on various parameters effect on the system operating. According to the mass fraction analysis, Pentane (0.5)/Butane (0.5) amongst the other mixtures has the best performance; due to this reason, this mixture is chosen to analyze in this section. Fig.10 (a) illustrates the varying of energy and exergy efficiency, net output power, and produced hydrogen with the different evaporating temperature of working fluid in Eva (1). The intended parameters have the same trend so that at the first step, the amounts of parameters rise with evaporation temperature increasing until a certain temperature ($380\ K$) and then start to reduce until the evaporation temperature of $390\ K$. The optimum values of first and second-law efficiency, net output power, and generated hydrogen by PEM electrolyzer are about $16.633\ \%$, $57.99\ \%$, $132.42\ kW$, $0.305\ kg/hr$, respectively. A similar parameter investigation of Eva (1) is performed for Eva (2), but as can be seen in Fig. 10 (b) the behavior of four parameters was different, the evaporation temperature of Eva (2) varied between $330\ K - 360\ K$ and the maximum point of net output power and produced hydrogen appears in $340\ K$ about $132.31\ K$, and $0.305\ kg/hr$, respectively. The first and second-law efficiency increase at the considered evaporation temperature ranges and varied between $15.97\% - 17.38\%$, and $56.95\% - 58.66\%$, respectively. The effect of the evaporator pinch point temperature as one of the main operational variables of the system for power and hydrogen

production is assessed, and the results are plotted in Fig. 10 (c), in this figure with increment of the pinch point temperature difference, the rate of power generation and hydrogen production as well as system performance criteria (energy and exergy efficiency) decrease. The evaporating temperature is known as one of the dominant factors that influence system performance significantly. Besides, the impacts of inlet cooling water temperatures to condensers on the system efficiency between certain values are evaluated and presented in Fig. 10 (d); the results show that the increment of the inlet cooling water temperature has an inverse impact on the system performance, and with increasing the inlet temperature of cooling water, the performance of the system drops.

3.3.Thermodynamic properties and optimization results

Thermodynamic parameters contain pressure, temperature, enthalpy, entropy, mass flow rate, as well as some other performance metrics at the base case condition, resulted from the mathematical assessments is represented in Tables 5 and 6. The results are analyzed for the mixture of Pentane (0.5)/Butane (0.5) because of its appropriate performance in comparison with other considered zeotropic combinations that were identified by the parametric analysis in past sections. Referring to Table 6, the energy and exergy efficiencies of the whole system are reported by about 16.66% and 58.03%, respectively. Also, the derived power from the proposed model and overall exergy destruction is calculated approximately $132.41\ kW$, and $90.08\ kW$, respectively. In addition, at the assumed condition, the geothermal heat source produces $0.306\ kg/h$ hydrogen by the proton exchange membrane electrolyzer. The Sankey diagram for the suggested geothermal flash cycle to show the exergy flow and destructed exergy for each component and states of the system is given in Fig. 11. The total exergy input to the system is estimated to be $\sim 225\ kW$, and the maximum and minimum exergy destruction of component is

obtained for the Steam turbine and pump (1), respectively. Besides, the amount of power production from high and low-pressure turbines and steam turbine are addressed about $10.59\ kW$, $25.16\ kW$, and $96.66\ kW$, respectively. The optimization process was done using the Genetic Algorithm for the Pentane/Butane mixture, in which the temperatures of evaporators 1 and 2 and also a mass fraction of zeotropic mixture are the decision value of this optimization, and the results are listed in Table 7. The results indicate that the best mass fractions for the intended mixture are 0.467 and 0.533 for Pentane and Butane, respectively. For this combination, the highest first and second-law efficiencies of the suggested system are about 16.67 %, and 58.14 %, respectively. The DORC unit power production and net output power of the entire system are about $36.2\ kW$, and $132.86\ kW$, respectively. The best hydrogen generation under GA optimization is approximately $0.3683\ kg/hr$.

4. Conclusion

In this paper, the application of renewable energy (geothermal) is implemented for power and hydrogen generation. A new hybrid system is proposed, including a geothermal flash cycle, DORC unit based on zeotropic mixtures with the aim of electricity production and proton exchange membrane electrolyzer for hydrogen production purposes. To enhance the DORC unit efficiency, zeotropic mixture as useful fluids is employed, so that the Pentane is combined with three various fluids: Butane, Cis-2-butene, and Trans-2-butene. Thermodynamic analysis has been developed by using the energy and exergy principles for the suggested system, and the optimization process was done applying the Genetic Algorithm. The main novelty and conclusions drawn from this study can be summarized below:

a. A new configuration of dual-pressure organic Rankine cycle and PEM electrolyzer as flash-binary cycles is integrated with a geothermal energy source.

b. To improve the proposed system performance, zeotropic mixtures are employed
c. The main usage of zeotropic mixtures is irreversibility reduction in the heating and cooling process that leads to efficiency improvement.
d. The mass fraction effect on the system performances for assumed zeotropic mixtures (Pentane/Butane, Pentane/Cis-2-butene, and Pentane/Trans-2-butene) is investigated so that the performance metrics of system (net output power, energy and exergy efficiencies, and produced hydrogen) with increment of mass fraction, increase to a maximum value and then decrease, the highest performance for flash-binary units and the whole system is mainly observed in the mass fraction range of [0.4-0.6].
e. The energy and exergy efficiencies of the whole system are reported by about 16.66% and 58.03% for the base case simulation.
f. The proposed system optimization is done using the Genetic Algorithm for the mixture of Pentane and Butane with the mass fractions of 0.467 and 0.533, respectively. The maximum thermal efficiency, exergy efficiency, and produced hydrogen for this mixture are reported about 16.66%, 58.03%, and $0.3683\ kg/hr$, respectively.

References:

[1] Wang N, Wang D, Xing Y, Shao L, Afzal S. Application of co-evolution RNA genetic algorithm for obtaining optimal parameters of SOFC model. Renewable Energy. 2020 Jan 1.

[2] Dincer I. Renewable energy and sustainable development: a crucial review. Renewable and sustainable energy reviews. 2000 Jun 1;4(2):157-75.

[3] Tchanche BF, Lambrinos G, Frangoudakis A, Papadakis G. Low-grade heat conversion into power using organic Rankine cycles–A review of various applications. Renewable and Sustainable Energy Reviews. 2011 Oct 1;15(8):3963-79.

[4] Shortall R, Davidsdottir B, Axelsson G. Geothermal energy for sustainable development: A review of sustainability impacts and assessment frameworks. Renewable and sustainable energy reviews. 2015 Apr 1;44:391-406.

[5] Yari M. Exergetic analysis of various types of geothermal power plants. Renewable energy. 2010 Jan 1;35(1):112-21.

[6] Jalilinasrabady S, Itoi R. Flash cycle and binary geothermal power plant optimization. InGeothermal Resources Council 2012 Annual Meeting, September 2012 Dec 1 (pp. 1079-1084).

[7] Coskun A, Bolatturk A, Kanoglu M. Thermodynamic and economic analysis and optimization of power cycles for a medium temperature geothermal resource. Energy conversion and management. 2014 Feb 1;78:39-49.

[8] Shokati N, Ranjbar F, Yari M. Comparative and parametric study of double flash and single flash/ORC combined cycles based on exergoeconomic criteria. Applied thermal engineering. 2015 Dec 5;91:479-95.

[9] Yilmaz C, Kanoglu M, Abusoglu A. Exergetic cost evaluation of hydrogen production powered by combined flash-binary geothermal power plant. International journal of hydrogen energy. 2015 Oct 26;40(40):14021-30.

[10] Zeyghami M. Performance analysis and binary working fluid selection of combined flash-binary geothermal cycle. Energy. 2015 Aug 1;88:765-74.

[11] Zhao Y, Wang J. Exergoeconomic analysis and optimization of a flash-binary geothermal power system. Applied energy. 2016 Oct 1;179:159-70.

[12] Venkatarathnam G, Mokashi G, Murthy SS. Occurrence of pinch points in condensers and evaporators for zeotropic refrigerant mixtures. International Journal of Refrigeration. 1996 Jul 1;19(6):361-8.

[13] Chys M, van den Broek M, Vanslambrouck B, De Paepe M. Potential of zeotropic mixtures as working fluids in organic Rankine cycles. Energy. 2012 Aug 1;44(1):623-32.

[14] Heberle F, Preißinger M, Brüggemann D. Zeotropic mixtures as working fluids in Organic Rankine Cycles for low-enthalpy geothermal resources. Renewable Energy. 2012 Jan 1;37(1):364-70.

[15] Lecompte S, Ameel B, Ziviani D, van den Broek M, De Paepe M. Exergy analysis of zeotropic mixtures as working fluids in Organic Rankine Cycles. Energy Conversion and Management. 2014 Sep 1;85:727-39.

[16] Radulovic J, Castaneda NI. On the potential of zeotropic mixtures in supercritical ORC powered by geothermal energy source. Energy conversion and management. 2014 Dec 1;88:365-71.

[17] Zhang J, Zhang H, Yang K, Yang F, Wang Z, Zhao G, Liu H, Wang E, Yao B. Performance analysis of regenerative organic Rankine cycle (RORC) using the pure working fluid and the zeotropic mixture over the whole operating range of a diesel engine. Energy conversion and management. 2014 Aug 1;84:282-94.

[18] Sadeghi M, Nemati A, Yari M. Thermodynamic analysis and multi-objective optimization of various ORC (organic Rankine cycle) configurations using zeotropic mixtures. Energy. 2016 Aug 15;109:791-802.

[19] Ho T, Mao SS, Greif R. Increased power production through enhancements to the Organic Flash Cycle (OFC). Energy. 2012 Sep 1;45(1):686-95.

[20] Kanoglu M. Exergy analysis of a dual-level binary geothermal power plant. Geothermics. 2002 Dec 1;31(6):709-24.

[21] Li J, Ge Z, Duan Y, Yang Z, Liu Q. Parametric optimization and thermodynamic performance comparison of single-pressure and dual-pressure evaporation organic Rankine cycles. Applied energy. 2018 May 1;217:409-21.

[22] Rostamzadeh H, Ebadollahi M, Ghaebi H, Shokri A. Comparative study of two novel micro-CCHP systems based on organic Rankine cycle and Kalina cycle. Energy conversion and management. 2019 Mar 1;183:210-29.

[23] Ni M, Leung MK, Leung DY. Energy and exergy analysis of hydrogen production by a proton exchange membrane (PEM) electrolyzer plant. Energy conversion and management. 2008 Oct 1;49(10):2748-56.

[24] Abdin Z, Webb CJ, Gray EM. Modelling and simulation of a proton exchange membrane (PEM) electrolyser cell. International Journal of Hydrogen Energy. 2015 Oct 19;40(39):13243-57.

[25] Ahmadi P, Dincer I, Rosen MA. Energy and exergy analyses of hydrogen production via solar-boosted ocean thermal energy conversion and PEM electrolysis. International Journal of Hydrogen Energy. 2013 Feb 12;38(4):1795-805.

[26] Lund JW, Freeston DH. World-wide direct uses of geothermal energy 2000. Geothermics. 2001 Feb 1;30(1):29-68.

[27] Kanoglu M, Bolatturk A. Performance and parametric investigation of a binary geothermal power plant by exergy. Renewable Energy. 2008 Nov 1;33(11):2366-74.

[28] Han J, Wang X, Xu J, Yi N, Talesh SS. Thermodynamic analysis and optimization of an innovative geothermal-based organic Rankine cycle using zeotropic mixtures for power and hydrogen production. International Journal of Hydrogen Energy. 2020 Mar 18;45(15):8282-99.

[29] Kanoglu M, Bolatturk A, Yilmaz C. Thermodynamic analysis of models used in hydrogen production by geothermal energy. International journal of hydrogen energy. 2010 Aug 1;35(16):8783-91.

[30] Ahmadi P, Dincer I, Rosen MA. Thermodynamic modeling and multi-objective evolutionary-based optimization of a new multigeneration energy system. Energy Conversion and Management. 2013 Dec 1;76:282-300.

[31] Ahmadi P, Dincer I, Rosen MA. Development and assessment of an integrated biomass-based multi-generation energy system. Energy. 2013 Jul 1;56:155-66.

[32] Miao, Di, et al. "Parameter estimation of PEM fuel cells employing the hybrid grey wolf optimization method." Energy 193 (2020): 116616.

[33] Santarelli MG, Torchio MF. Experimental analysis of the effects of the operating variables on the performance of a single PEMFC. Energy Conversion and Management. 2007 Jan 1;48(1):40-51.

[34] Gurau V, Barbir F, Liu H. An analytical solution of a half-cell Model for PEM fuel cells. Journal of the Electrochemical Society. 2000 Jul 1;147(7):2468-77.

[35] Man KF, Tang KS, Kwong S. Genetic algorithms: Concept and design.

[36] Goldberg, David E. "Genetic algorithms in search." Optimization, and MachineLearning (1989).

[37] Deb, Kalyanmoy. "An introduction to genetic algorithms." Sadhana 24.4-5 (1999): 293-315.

[38] Balasubramanian, Karthik, et al. "Critical evaluation of genetic algorithm based fuel cell parameter extraction." Energy Procedia 75 (2015): 1975-1982.

[39] Qiu, Meikang, et al. "Phase-change memory optimization for green cloud with genetic algorithm." IEEE Transactions on Computers 64.12 (2015): 3528-3540.

[40] Shah RK, Sekulic DP. Fundamentals of heat exchanger design. John Wiley & Sons; 2003 Aug 11.

[41] Yilmaz C, Kanoglu M, Abusoglu A. Exergetic cost evaluation of hydrogen production powered by combined flash-binary geothermal power plant. International journal of hydrogen energy. 2015 Oct 26;40(40):14021-30.

[42] Li J, Ge Z, Duan Y, Yang Z. Effects of heat source temperature and mixture composition on the combined superiority of dual-pressure evaporation organic Rankine cycle and zeotropic mixtures. Energy. 2019 May 1;174:436-49..

[43] Ioroi T, Yasuda K, Siroma Z, Fujiwara N, Miyazaki Y. Thin film electrocatalyst layer for unitized regenerative polymer electrolyte fuel cells. Journal of Power sources. 2002 Nov 14;112(2):583-7.

Figures:

Fig. 1. Schematic diagram of proposed combined system.

Fig. 2. $T - s$ diagram for the dual-pressure organic Rankine cycle.

Fig. 3. Flowchart of Genetic algorithm.

Fig. 4. Comparison of the present simulation results with the Li et al.[42] obtained data for DORC unit.

Fig. 5. Comparison of the present simulation results with Ref.[43] obtained data for PEM electrolyzer system.

Fig. 6. Comparison of the present simulation results with Ref.[41] obtained data for geothermal flash cycle system .

Fig. 7. Effect of mass fraction (m_f) on (a) mass flow rate of DORC unit, (b) output work of DORC unit, (c) total net output work, (d) energy efficiency of DRC unit, (e) energy efficiency of entire system, (f) the rate of hydrogen production.

Fig. 8. Effect of mass fraction (m_f) on the exergy destruction rate of each components of proposed system.

Fig. 9. Effect of mass fraction (m_f) on the rate of exergy destruction and exergy efficiency of DORC unit and entire system.

Fig. 10. The trend of variation for different performance parameters with $T_{evaporation}$ (1) and (2), $\Delta T_{pp,eva}$ and inlet temperature of cooling water for various working fluids.

Fig. 11. The Sankey diagram of proposed flash-binary geothermal system

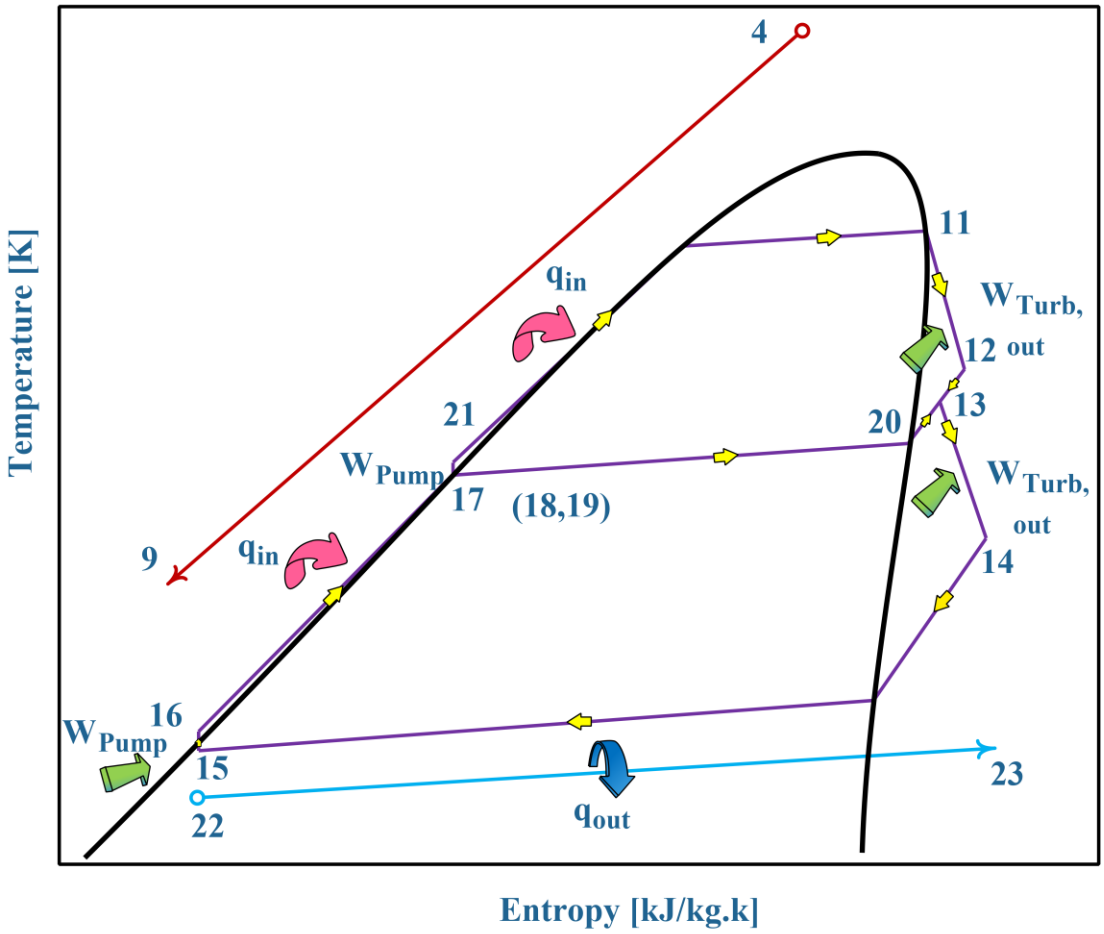
4
11
q_{in}
$W_{Turb,}$
12 out
21
20
13
W_{Pump}
17
(18,19)
$W_{Turb,}$
out
9
q_{in}
14
16
W_{Pump}
15
23
22
q_{out}
Temperature [K]
Entropy [kJ/kg.k]

Figure 1

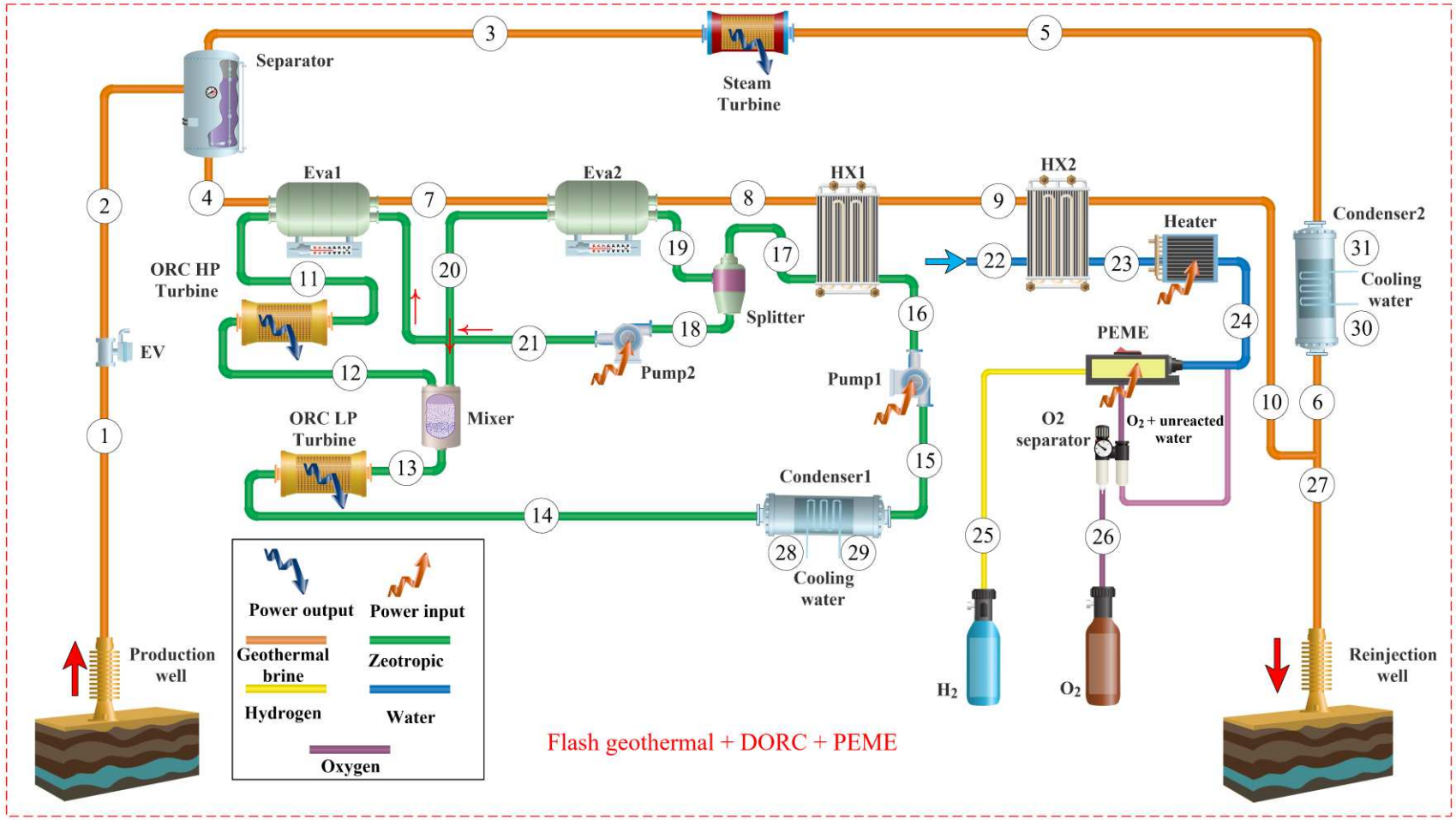
Separator
Steam Turbine
Eva1
Eva2
HX1
HX2
Heater
Condenser2
Cooling water
ORC HP Turbine
EV
Splitter
Pump2
Pump1
PEME
O2 separator
O2 + unreacted water
ORC LP Turbine
Mixer
Condenser1
Cooling water
Production well
Reinjection well
H2
O2
Power output
Power input
Geothermal brine
Zeotropic
Hydrogen
Water
Oxygen
Flash geothermal + DORC + PEME

Figure 2

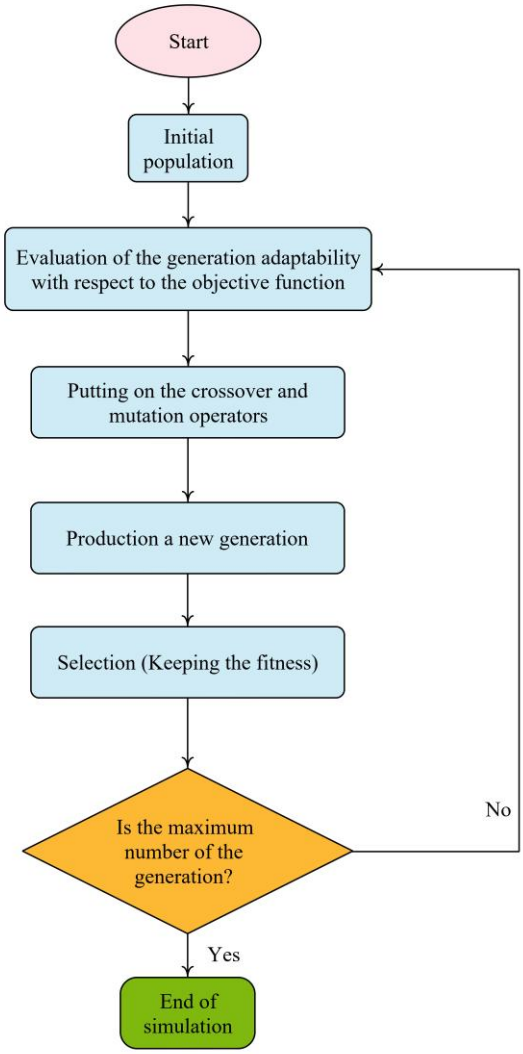
Start
Initial population
Evaluation of the generation adaptability with respect to the objective function
Putting on the crossover and mutation operators
Production a new generation
Selection (Keeping the fitness)
Is the maximum number of the generation?
No
Yes
End of simulation

Figure 3

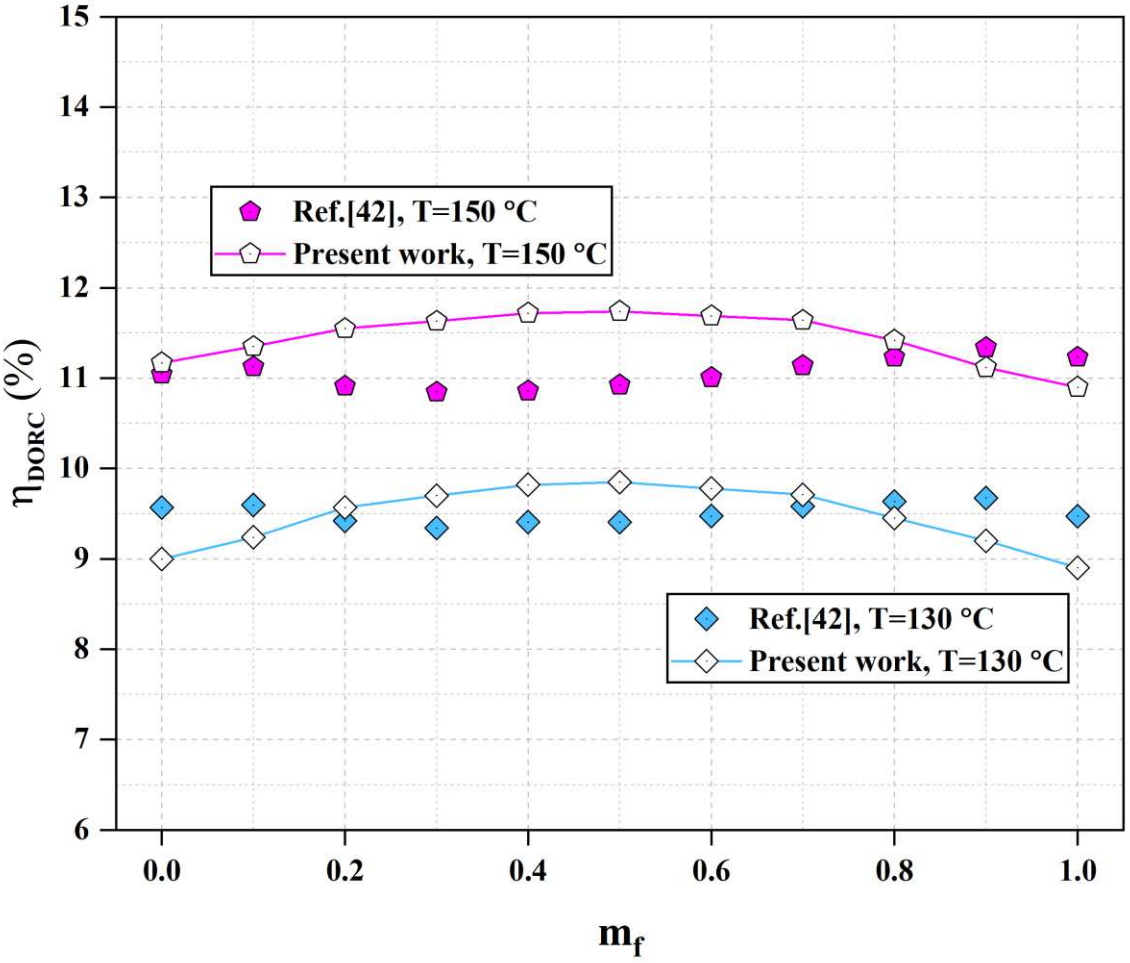
15
14
13
12
11
10
9
8
7
6
0.0
0.2
0.4
0.6
0.8
1.0
η_{DORC} (%)
m_f
Ref.[42], T=150 °C
Present work, T=150 °C
Ref.[42], T=130 °C
Present work, T=130 °C

Figure 4

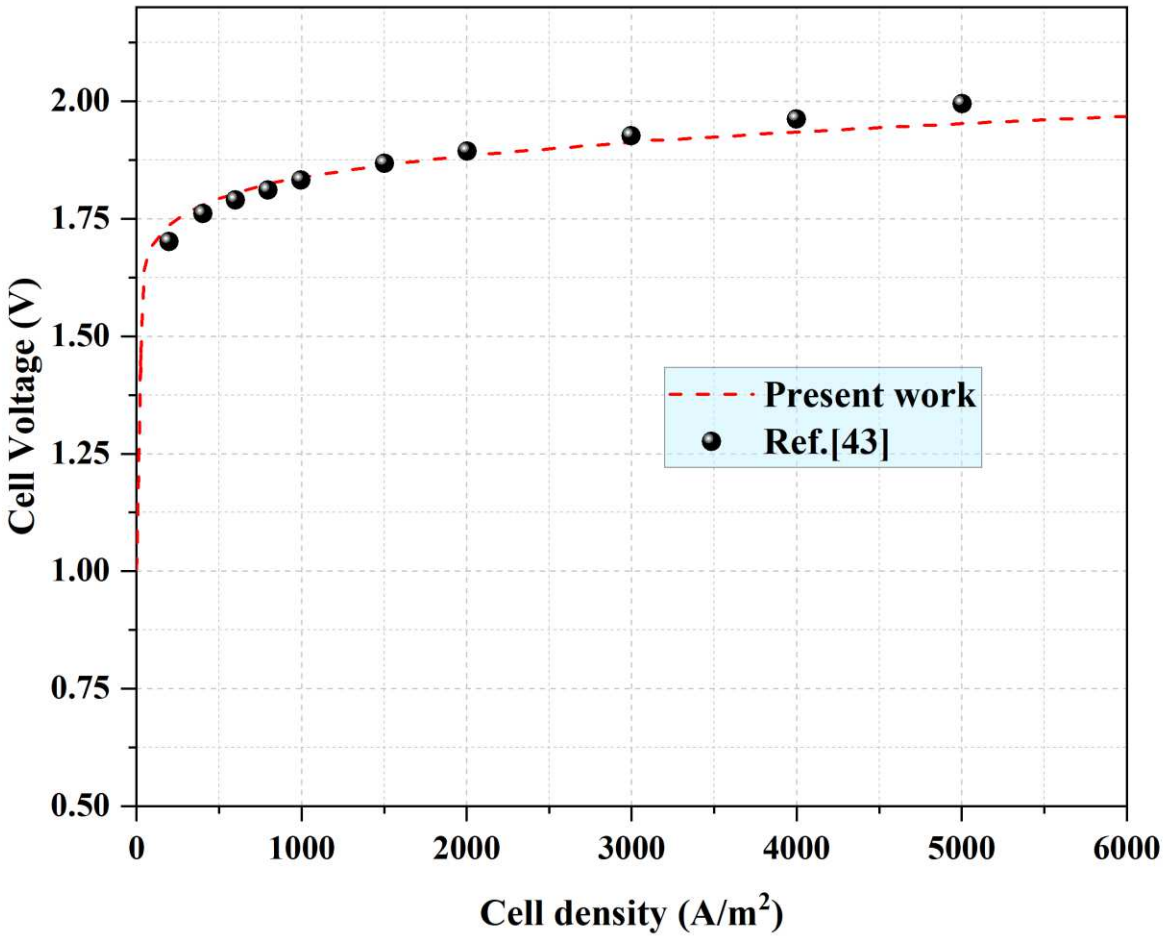
2.00
1.75
1.50
1.25
1.00
0.75
0.50
Cell Voltage (V)
0
1000
2000
3000
4000
5000
6000
Cell density (A/m^2)
Present work
Ref.[43]

Figure 5

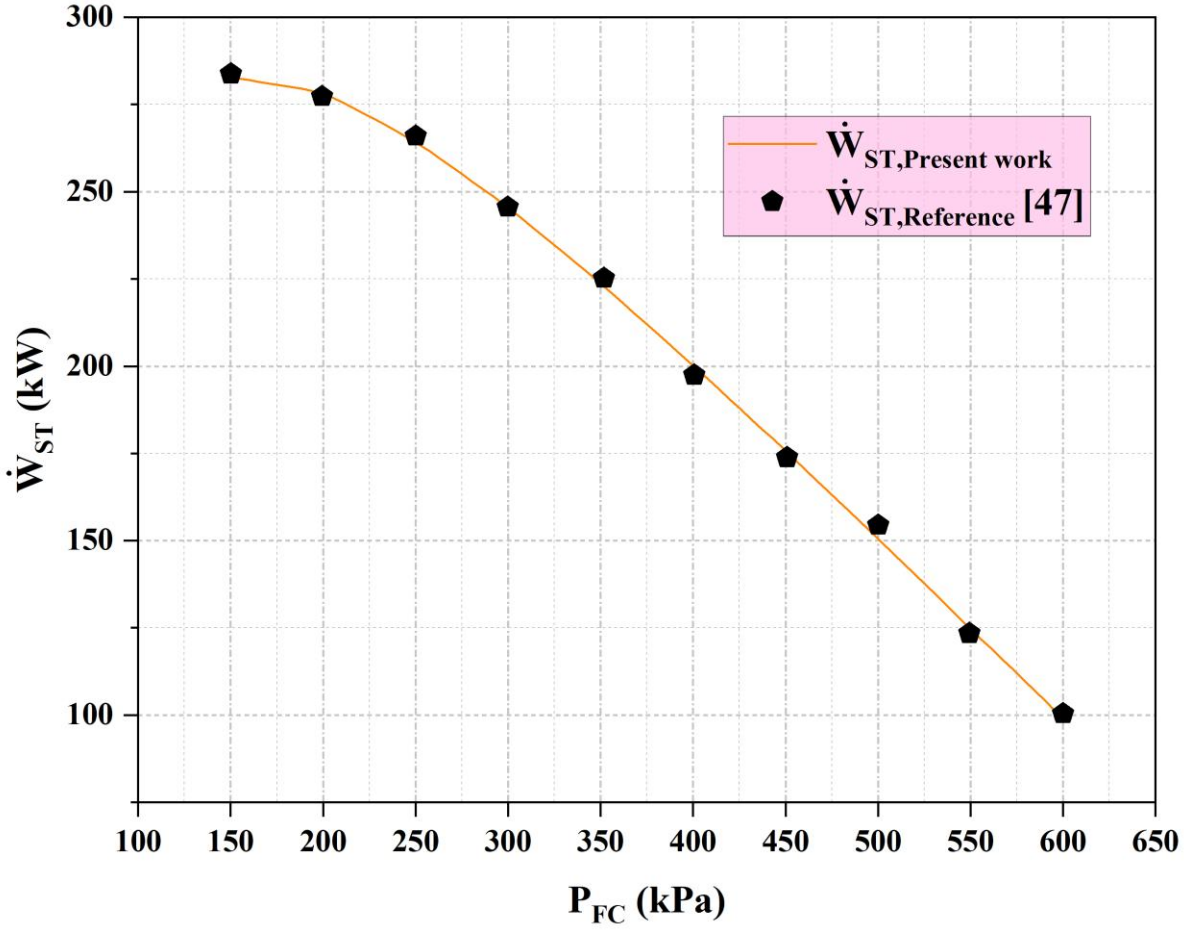
300
250
200
150
100
$\dot{W}_{ST}$ (kW)
100
150
200
250
300
350
400
450
500
550
600
650
P_{FC} (kPa)
$\dot{W}_{ST,Present\ work}$
$\dot{W}_{ST,Reference}$ [47]

Figure 6

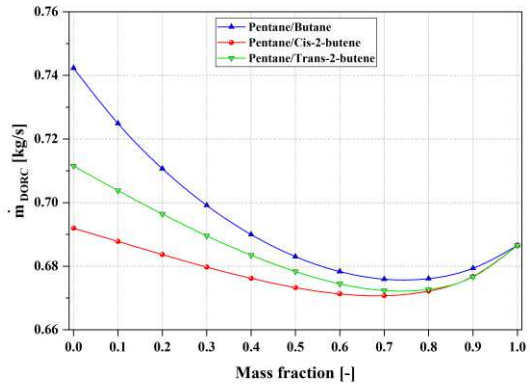

(a)

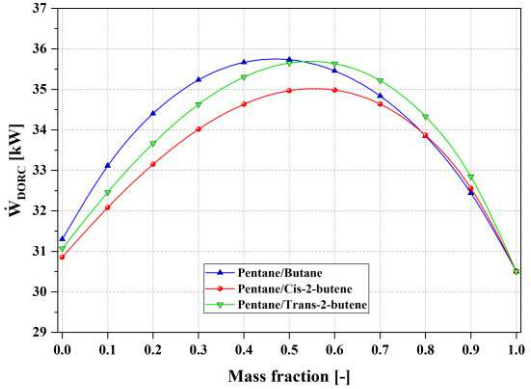

(b)

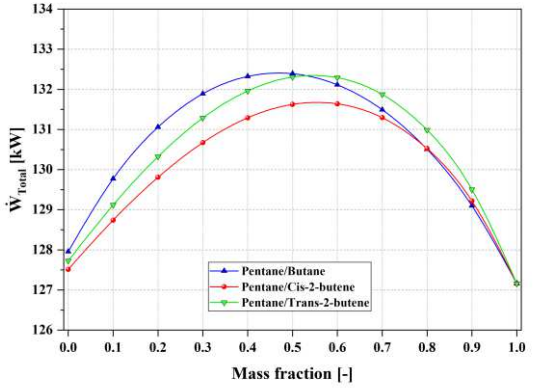

(c)

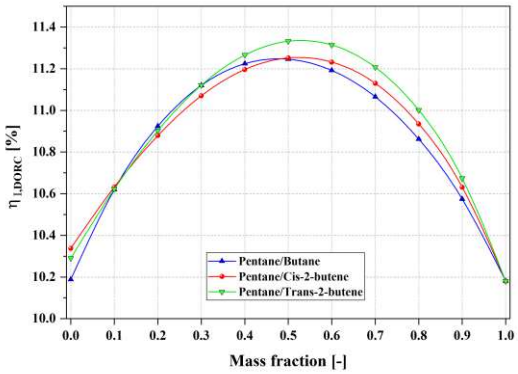

(d)

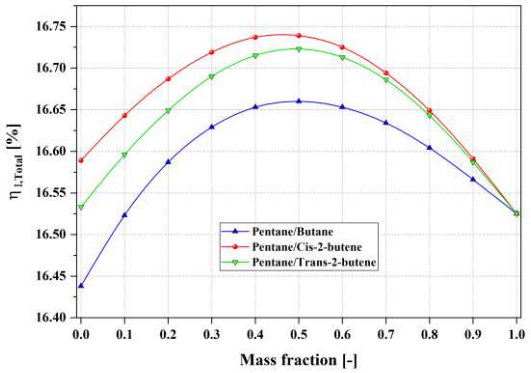

(e)

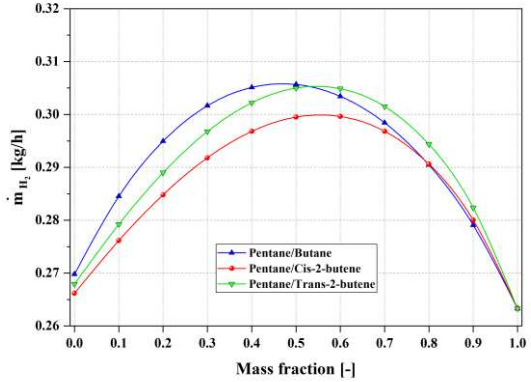

(f)

Figure 7

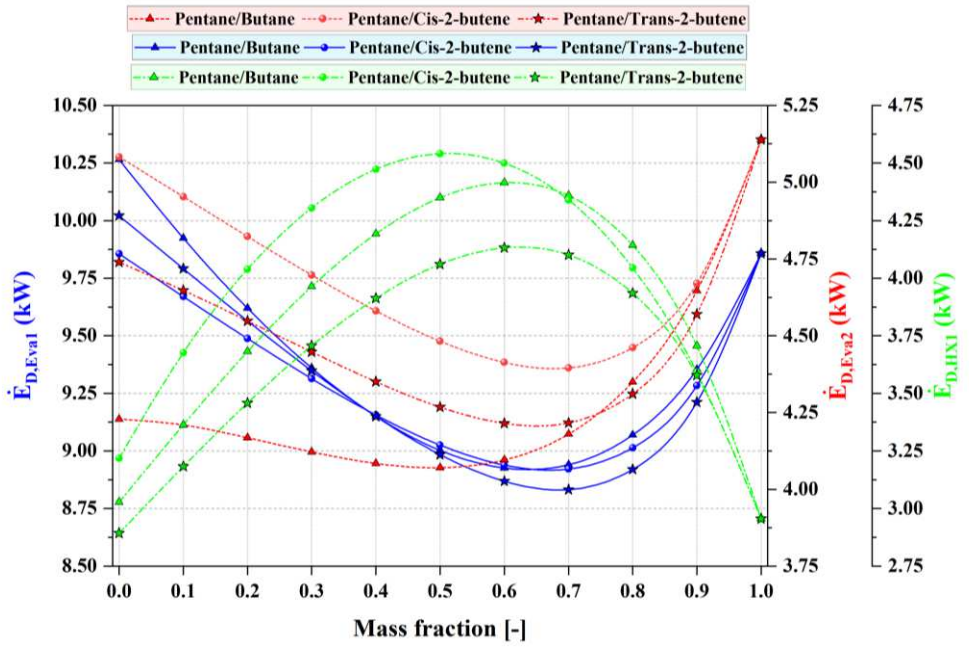
Pentane/Butane
Pentane/Cis-2-butene
Pentane/Trans-2-butene
Pentane/Butane
Pentane/Cis-2-butene
Pentane/Trans-2-butene
Pentane/Butane
Pentane/Cis-2-butene
Pentane/Trans-2-butene
$\dot{E}_{D,Eva1}$ (kW)
$\dot{E}_{D,Eva2}$ (kW)
$\dot{E}_{D,HX1}$ (kW)
Mass fraction [-]

(a)

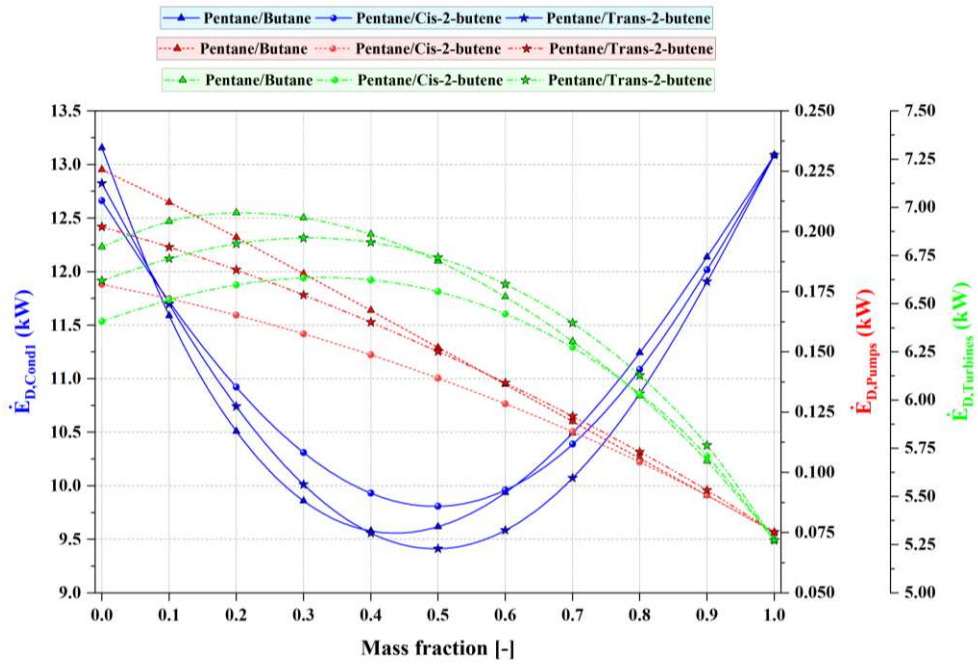
Pentane/Butane
Pentane/Cis-2-butene
Pentane/Trans-2-butene
Pentane/Butane
Pentane/Cis-2-butene
Pentane/Trans-2-butene
Pentane/Butane
Pentane/Cis-2-butene
Pentane/Trans-2-butene
$\dot{E}_{D,Cond1}$ (kW)
$\dot{E}_{D,Pumps}$ (kW)
$\dot{E}_{D,Turbines}$ (kW)
Mass fraction [-]

(b)

Figure 8

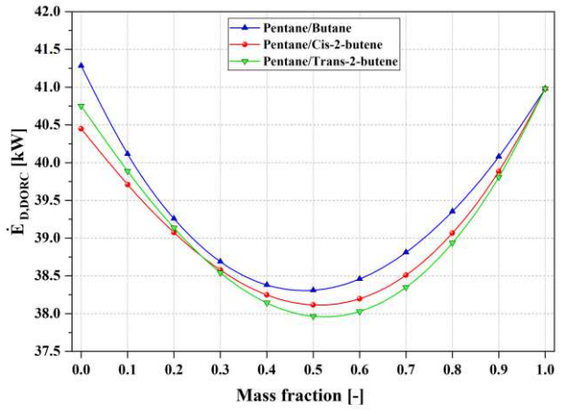

(a)

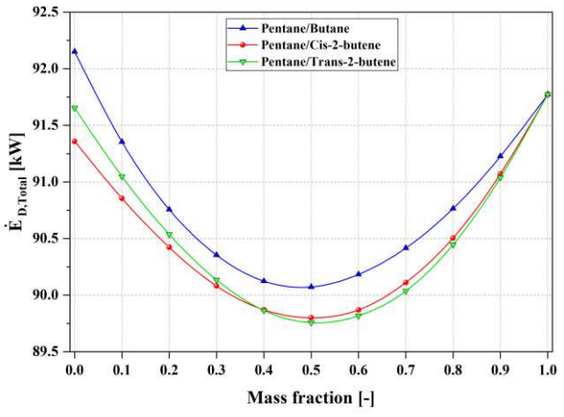

(b)

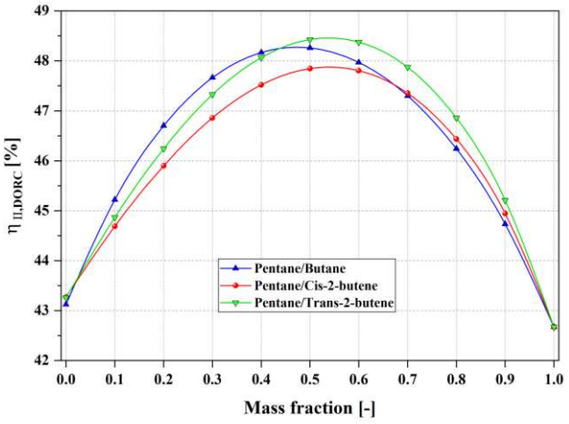

(c)

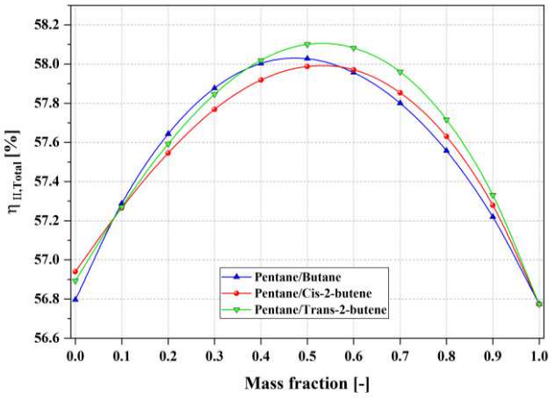

(d)

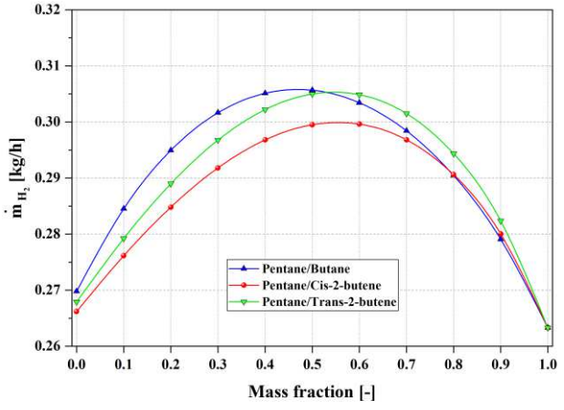

(e)

Figure 9

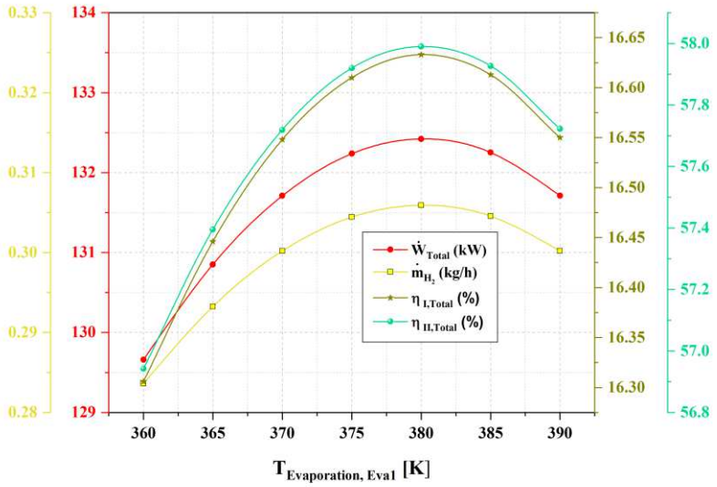

(a)

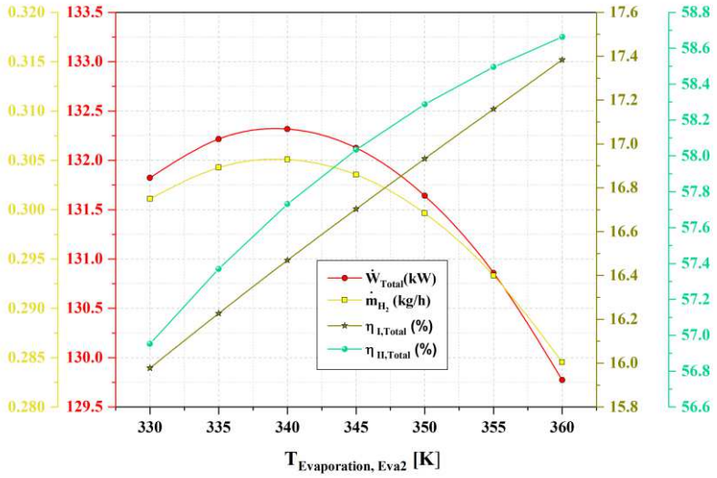

(b)

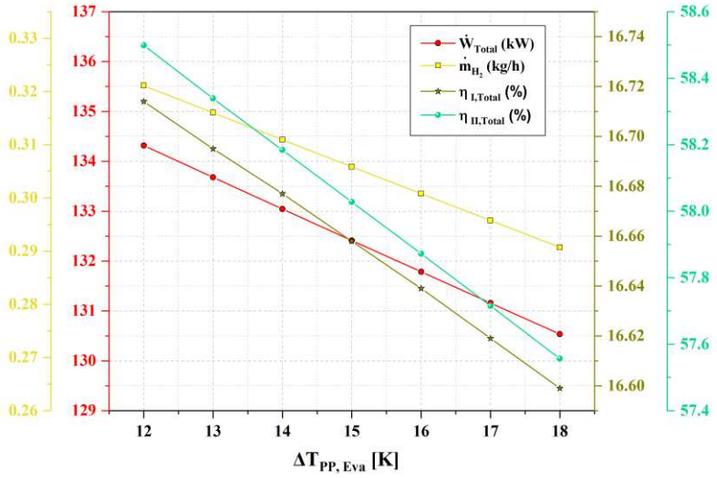

(b)

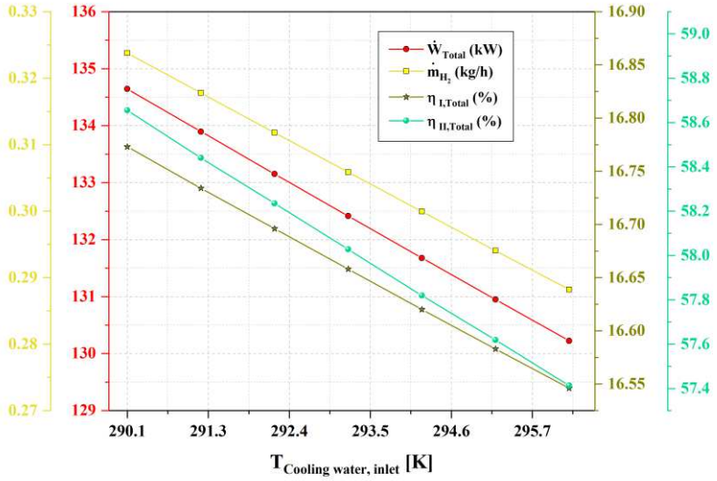

(d)

Figure 10

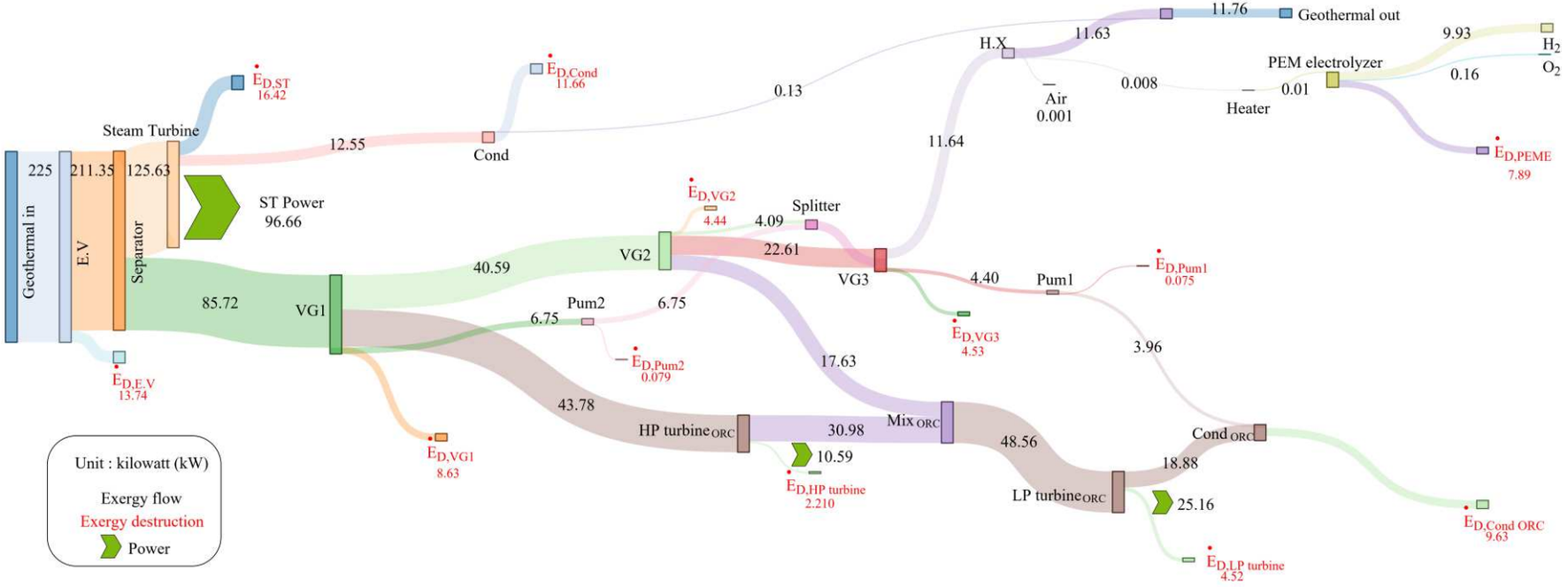
Geothermal in
225
E.V
211.35
Separator
125.63
85.72
Steam Turbine
ST Power
96.66
E_D,ST
16.42
12.55
Cond
E_D,Cond
11.66
0.13
11.76
Geothermal out
H.X
11.63
11.64
Air
0.001
0.008
Heater
0.01
PEM electrolyzer
9.93
H2
O2
0.16
E_D,PEME
7.89
VG1
40.59
VG2
E_D,VG2
4.44
4.09
Splitter
22.61
VG3
4.40
Pum1
E_D,Pum1
0.075
E_D,VG3
4.53
3.96
Pum2
6.75
6.75
E_D,Pum2
0.079
E_D,VG1
8.63
43.78
17.63
HP turbine ORC
30.98
10.59
E_D,HP turbine
2.210
Mix ORC
48.56
LP turbine ORC
18.88
25.16
Cond ORC
E_D,Cond ORC
9.63
E_D,LP turbine
4.52
E_D,E.V
13.74
Unit : kilowatt (kW)
Exergy flow
Exergy destruction
Power

Figure 11

Tables:

Table 1. The properties of the zeotropic mixtures.

Fluid	$T_{cr}\ (K)$	$P_{cr}\ (MPa)$	$MM\ (g/mol)$	$D\ (kg/m^3)$	$Cp(kJ/kg\ K)$	$C\ (W/m\ K)$	ODP	$GWP\ (year)$	$Type\ (\frac{dT}{ds})$
Pentane	469.7	3.37	72.149	556.04	2.64	0.091	0	2	Dry
Butane	425.13	3.80	58.122	490.23	2.92	0.082	0	3	Dry
Cis-2-butane	435.75	4.23	56.106	532.81	2.63	0.087	0	2	Dry
Trans-2-butane	428.61	4.03	56.106	514.11	2.76	0.085	N.A	N.A	Dry

Table 2. Assumed values of the proposed system

Parameter	Symbol	Value	Unit
Geothermal unit inputs			
Mass flow rate of geothermal fluid	$\dot{m}_1$	1	$kg.s^{-1}$
Geothermal fluid enthalpy	h_1	1000	$kJ.kg^{-1}$
Geothermal fluid temperature	T_1	461.11	K
Geothermal fluid pressure	P_1	1200	kPa
Flash chamber pressure	P_2	550	kPa
Steam turbine pressure ratio	r_p	120	$-$
Inputs of dual-pressure organic Rankine cycle based on zeotropic mixtures			
Efficiency of the turbine	η_T	85	%
Efficiency of the pump	η_p	85	%
Inlet temperature of the cooling water	T_c	293.15	K
Inlet pressure of the cooling water	P_c	150	kPa
Condenser pinch point temperature difference	$\Delta T_{PP,Cond}$	10	K
Evaporaotrs pinch point temperature difference	$\Delta T_{PP,Eva}$	15	K
pinch point temperature difference of Heat exchanger (1)	$\Delta T_{PP,H.X(1)}$	15	K
pinch point temperature difference of Heat exchanger (2)	$\Delta T_{PP,H.X\,(2)}$	10	K

Input parameters of the proton exchange membrane electrolyzer			
Oxygen pressure	P_{O_2}	100	kPa
Hydrogen pressure	P_{H_2}	100	kPa
PEM electrolyzer working temperature	T_{PEM}	353.15	K
Anode activation energy	$E_{act,a}$	76	$(kJ.mol^{-1})$
Cathode activation energy	$E_{act,c}$	18	$(kJ.mol^{-1})$
Water content at the anode-membrane interface	λ_a	14	Ω^{-1}
Water content at the anode-membrane interface	λ_c	10	Ω^{-1}
Membrane thickness	D	100	μm
pre-exponential factor for anode	j_a^{ref}	$1.7E5$	$A.m^{-2}$
pre-exponential factor for cathode	j_c^{ref}	$4.6E3$	$A.m^{-2}$
Faraday constant	F	98486	$C.mol^{-1}$

Table 3. Mass and energy conservation relations for the components of the devised system

Component	Mass balance equation	Energy balance equation
Expansion valve (E.V.)	$\dot{m}_1 = \dot{m}_2$	$\dot{m}_1 h_1 = \dot{m}_2 h_2$
Separator	$\dot{m}_2 = \dot{m}_3 + \dot{m}_4$	$\dot{m}_2 h_2 = \dot{m}_3 h_3 + \dot{m}_4 h_4$
Steam turbine	$\dot{m}_3 = \dot{m}_5$	$\dot{W}_{ST} = \dot{m}_3 h_3 - \dot{m}_5 h_5 = (\dot{m}_3 h_3 - \dot{m}_5 h_{5s})\eta_{ST}$
Condenser 2 (Cond 2)	$\dot{m}_5 = \dot{m}_6, \dot{m}_{30} = \dot{m}_{31}$	$\dot{Q}_{Cond2} = \dot{m}_5 h_5 - \dot{m}_6 h_6 = \dot{m}_{31} h_{31} - \dot{m}_{30} h_{30}$
Evaporator 1 (Eva1)	$\dot{m}_4 = \dot{m}_7, \dot{m}_{21} = \dot{m}_{11}$	$\dot{Q}_{Eva1} = \dot{m}_4 h_4 - \dot{m}_7 h_7 = \dot{m}_{11} h_{11} - \dot{m}_{21} h_{21}$
Evaporator 2 (Eva2)	$\dot{m}_7 = \dot{m}_8, \dot{m}_{20} = \dot{m}_{19}$	$\dot{Q}_{Eva2} = \dot{m}_7 h_7 - \dot{m}_8 h_8 = \dot{m}_{20} h_{20} - \dot{m}_{19} h_{19}$
Heat exchanger 1 (HX 1)	$\dot{m}_8 = \dot{m}_9, \dot{m}_{17} = \dot{m}_{16}$	$\dot{Q}_{Hx1} = \dot{m}_8 h_8 - \dot{m}_9 h_9 = \dot{m}_{17} h_{17} - \dot{m}_{16} h_{16}$
HP Turbine (HP,tur)	$\dot{m}_{11} = \dot{m}_{12}$	$\dot{W}_{\text{HP,tur}} = \dot{m}_{11} h_{11} - \dot{m}_{12} h_{12} = (\dot{m}_{11} h_{11} - \dot{m}_{12} h_{12s})\eta_T$
LP Turbine (LP,tur)	$\dot{m}_{13} = \dot{m}_{14}$	$\dot{W}_{\text{LP,tur}} = \dot{m}_{13} h_{13} - \dot{m}_{14} h_{14} = (\dot{m}_{13} h_{13} - \dot{m}_{14} h_{14s})\eta_T$
HP Pump (HP,pump)	$\dot{m}_{21} = \dot{m}_{18}$	$\dot{W}_{\text{HP,pump}} = \dot{m}_{21} h_{21} - \dot{m}_{18} h_{18} = (\dot{m}_{21} h_{21s} - \dot{m}_{18} h_{18})/\eta_p$
LP Pump (LP,pump)	$\dot{m}_{16} = \dot{m}_{15}$	$\dot{W}_{\text{LP,pump}} = \dot{m}_{16} h_{16} - \dot{m}_{15} h_{15} = (\dot{m}_{16} h_{16s} - \dot{m}_{15} h_{15})/\eta_p$
Condenser 1 (Cond1)	$\dot{m}_{14} = \dot{m}_{15}, \dot{m}_{29} = \dot{m}_{28}$	$\dot{Q}_{Cond1} = \dot{m}_{14} h_{14} - \dot{m}_{15} h_{15} = \dot{m}_{29} h_{29} - \dot{m}_{28} h_{28}$

Heat exchanger 2 (H.X 2)	$\dot{m}_9 = \dot{m}_{10}, \dot{m}_{23} = \dot{m}_{22}$	$\dot{Q}_{\text{H.X.}} = \dot{m}_9 h_9 - \dot{m}_{10} h_{10} = \dot{m}_{23} h_{23} - \dot{m}_{22} h_{22}$
Heater (Heater)	$\dot{m}_{24} = \dot{m}_{23}$	$\dot{W}_{\text{Heater}} = \dot{m}_{24} h_{24} - \dot{m}_{23} h_{23}$
Electrolyzer (Electro)	$\dot{m}_{\text{Electro},in} = \dot{m}_{25} + \dot{m}_{26} + \dot{m}_{Electro,out}$	$\dot{W}_{\text{Electro},in} = JV$

Table 4. Exergy metrics for each component of the devised system

Component	**Fuel Exergy**	**Product Exergy**	**Exergy destruction**	**Exergy efficiency**
Expansion valve (E.V.)	$\dot{E}_F^{E.V} = \dot{E}_1$	$\dot{E}_P^{E.V} = \dot{E}_2$	$\dot{E}_D^{E.V} = \dot{E}_F^{E.V} - \dot{E}_P^{E.V}$	$\dot{E}_P^{E.V} / \dot{E}_F^{E.V}$
Separator (Sep)	$\dot{E}_F^{Sep} = \dot{E}_2$	$\dot{E}_P^{Sep} = \dot{E}_3 + \dot{E}_4$	$\dot{E}_D^{Sep} = \dot{E}_F^{Sep} - \dot{E}_P^{Sep}$	$\dot{E}_P^{Sep} / \dot{E}_F^{Sep}$
Steam turbine (ST)	$\dot{E}_F^{ST} = \dot{E}_3 - \dot{E}_5$	$\dot{E}_P^{ST} = \dot{W}_{ST}$	$\dot{E}_D^{ST} = \dot{E}_F^{ST} - \dot{E}_P^{ST}$	$\dot{E}_P^{ST} / \dot{E}_F^{ST}$

Condenser 2 (Cond 2)	$\dot{E}_F^{Cond2} = \dot{E}_5 - \dot{E}_6$	$\dot{E}_P^{Cond2} = \dot{E}_{31} - \dot{E}_{30}$	$\dot{E}_D^{Cond2} = \dot{E}_F^{Cond2} - \dot{E}_P^{Cond2}$	$\dot{E}_P^{Cond2}/\dot{E}_F^{Cond2}$
Evaporator (Eva1)	$\dot{E}_F^{Eva\ 1} = \dot{E}_4 - \dot{E}_7$	$\dot{E}_P^{Eva1} = \dot{E}_{11} - \dot{E}_{21}$	$\dot{E}_D^{Eva1} = \dot{E}_F^{Eva1} - \dot{E}_P^{Eva1}$	$\dot{E}_P^{Eva1}/\dot{E}_F^{Eva1}$
Evaporator (Eva 2)	$\dot{E}_F^{Eva\ 2} = \dot{E}_7 - \dot{E}_8$	$\dot{E}_P^{Eva2} = \dot{E}_{20} - \dot{E}_{19}$	$\dot{E}_D^{Eva2} = \dot{E}_F^{Eva2} - \dot{E}_P^{Gen2}$	$\dot{E}_P^{Eva2}/\dot{E}_F^{Eva2}$
Heat Exchanger (H.X. 1)	$\dot{E}_F^{H.X1} = \dot{E}_8 - \dot{E}_9$	$\dot{E}_P^{H.X1} = \dot{E}_{17} - \dot{E}_{16}$	$\dot{E}_D^{H.X1} = \dot{E}_F^{H.X1} - \dot{E}_P^{H.X1}$	$\dot{E}_P^{H.X1}/\dot{E}_F^{H.X1}$
HP Turbine (HP,tur)	$\dot{E}_F^{\mathrm{HP,tur}} = \dot{E}_{11} - \dot{E}_{12}$	$\dot{E}_P^{\mathrm{HP,tur}} = \dot{W}_{\mathrm{HP,tur}}$	$\dot{E}_D^{\mathrm{HP,tur}} = \dot{E}_F^{\mathrm{HP,tur}} - \dot{E}_P^{\mathrm{HP,tur}}$	$\dot{E}_P^{\mathrm{HP,tur}}/\dot{E}_F^{\mathrm{HP,tur}}$
LP Turbine (LP,tur)	$\dot{E}_F^{\mathrm{LP,tur}} = \dot{E}_{13} - \dot{E}_{14}$	$\dot{E}_P^{\mathrm{LP,tur}} = \dot{W}_{\mathrm{LP,tur}}$	$\dot{E}_D^{\mathrm{LP,tur}} = \dot{E}_F^{\mathrm{LP,tur}} - \dot{E}_P^{\mathrm{LP,tur}}$	$\dot{E}_P^{\mathrm{LP,tur}}/\dot{E}_F^{\mathrm{LP,tur}}$
HP Pump (HP,pump)	$\dot{E}_F^{\mathrm{HP,pump}} = \dot{W}_{\mathrm{HP,pump}}$	$\dot{E}_P^{\mathrm{HP,pump}} = \dot{E}_{21} - \dot{E}_{18}$	$\dot{E}_D^{\mathrm{HP,pump}} = \dot{E}_F^{\mathrm{HP,pump}} - \dot{E}_P^{\mathrm{HP,pump}}$	$\dot{E}_P^{\mathrm{HP,pump}}/\dot{E}_F^{\mathrm{HP,pump}}$
LP Pump (LP,pump)	$\dot{E}_F^{\mathrm{LP,pump}} = \dot{W}_{\mathrm{LP,pump}}$	$\dot{E}_P^{\mathrm{LP,pump}} = \dot{E}_{16} - \dot{E}_{15}$	$\dot{E}_D^{\mathrm{LP,pump}} = \dot{E}_F^{\mathrm{LP,pump}} - \dot{E}_P^{\mathrm{LP,pump}}$	$\dot{E}_P^{\mathrm{LP,pump}}/\dot{E}_F^{\mathrm{LP,pump}}$
Condenser 1 (Cond 1)	$\dot{E}_F^{Cond1} = \dot{E}_{14} - \dot{E}_{15}$	$\dot{E}_P^{Cond1} = \dot{E}_{29} - \dot{E}_{28}$	$\dot{E}_D^{Cond1} = \dot{E}_F^{Cond1} - \dot{E}_P^{Cond1}$	$\dot{E}_P^{Cond1}/\dot{E}_F^{Cond1}$
Heat exchanger (H.X. 2)	$\dot{E}_F^{\mathrm{H.X\ 2}} = \dot{E}_9 - \dot{E}_{10}$	$\dot{E}_P^{\mathrm{H.X\ 2}} = \dot{E}_{23} - \dot{E}_{22}$	$\dot{E}_D^{\mathrm{H.X\ 2}} = \dot{E}_F^{\mathrm{H.X\ 2}} - \dot{E}_P^{\mathrm{.H.X\ 2}}$	$\dot{E}_P^{\mathrm{H.X\ 2}}/\dot{E}_F^{\mathrm{H.X\ 2}}$
Heater (Heater)	$\dot{E}_F^{\mathrm{Heater}} = \dot{W}_{\mathrm{Heater}}$	$\dot{E}_P^{\mathrm{Heater}} = \dot{E}_{24} - \dot{E}_{23}$	$\dot{E}_D^{\mathrm{Heater}} = \dot{E}_F^{\mathrm{Heater}} - \dot{E}_P^{\mathrm{Heater}}$	$\dot{E}_P^{\mathrm{Heater}}/\dot{E}_F^{\mathrm{Heater}}$
Electrolyzer (Electro)	$\dot{E}_F^{\mathrm{Electro}} = \dot{W}_{\mathrm{Electro},in}$	$\dot{E}_P^{\mathrm{Electro}} = \dot{E}_{25} + \dot{E}_{26}$	$\dot{E}_D^{\mathrm{Electro}} = \dot{E}_F^{\mathrm{Electro}} - \dot{E}_P^{\mathrm{Electro}}$	$\dot{E}_P^{\mathrm{Electro}}/\dot{E}_F^{\mathrm{Electro}}$

Table 5. State point properties in the base conditions for mixture of Pentane (0.5)/Butane (0.5)

State	$T(K)$	$P(kPa)$	$h(kj/kg)$	$s(\frac{kj}{kg.K})$	$\dot{E}$(kW)	$\dot{m}$(kg/s)
1	461.11	1200	1000	2.653	225.09	1
2	428.61	550	1000	2.70	211.35	1
3	428.61	550	2752.33	6.789	125.63	0.16
4	428.61	550	655.76	1.897	85.72	0.84
5	304.48	4.58	2163.64	7.13	12.55	0.16
6	304.48	4.58	131.31	0.455	0.13	0.16
7	382.93	550	460.80	1.416	40.6	0.84
8	358.50	550	357.87	1.138	22.62	0.84
9	338.82	550	275.34	0.902	11.65	0.84
10	338.78	550	275.20	0.901	11.63	0.84
11	387.37	1229.74	615.47	2.018	43.79	0.426
12	363.83	567.08	589.15	2.031	30.99	0.426
13	359.53	567.08	580.04	2.006	48.57	0.684
14	333.25	191.65	542.46	2.026	18.88	0.684
15	303.17	191.65	129.54	0.692	3.97	0.684
16	303.36	567.08	130.3	0.692	4.41	0.684
17	343.5	567.08	231.23	1.004	10.85	0.684

18	343.5	567.08	231.23	1.004	6.76	0.426
19	343.5	567.08	231.23	1.004	4.09	0.258
20	352.4	567.08	564.99	1.963	17.63	0.258
21	343.96	1229.74	232.68	1.005	7.72	0.426
22	293.15	101	84.01	0.296	-	0.00076
23	328.82	101	233.11	0.776	0.01	0.00076
24	353	101	334.43	1.074	0.02	0.00076
25	353	101	4720.43	55.816	9.93	0.000085
26	353	101	321.71	6.564	0.17	0.000675
27	333.23	20.03	251.58	0.832	10.47	1

Table 6. Performance criteria of the new suggested cycle for a mixture of Pentane/Butane in base condition

Parameter	Present work
$\dot{W}_{Total}\ (kW)$	132.41
$\dot{W}_{DORC}\ (kW)$	35.76
$\dot{W}_{Electro,in}\ (kW)$	17.88
$\eta_{I,Total}(\%)$	16.66
$\eta_{I,DORC}(\%)$	11.25
$\eta_{I,PEM}(\%)$	56.53
$\eta_{II,tot}(\%)$	58.03

$\eta_{II,DORC}(\%)$	48.27
$\eta_{II,PEM}(\%)$	56.10
$\dot{E}_{D,Total}$(kW)	90.08
$\dot{E}_{D,DORC}$(kW)	38.32
$\dot{E}_{D,PEM}$(kW)	7.89
$\dot{m}_{H_2}$(kg/h)	0.306

Table 7. Optimization result of the new suggested cycle for a mixture of Pentane/Butane

Parameter	Present work
$\dot{W}_{Total}\ (kW)$	132.86
$\dot{W}_{DORC}\ (kW)$	36.2
$\dot{W}_{Electro,in}\ (kW)$	18.1
$\eta_{I,Total}(\%)$	16.67
$\eta_{I,DORC}(\%)$	11.34
$\eta_{I,PEM}(\%)$	56.48
$\eta_{II,tot}(\%)$	58.14
$\eta_{II,ORC}(\%)$	48.75

$\eta_{II,PEM}(\%)$	56.05
$\dot{E}_{D,Total}$(kW)	89.91
$\dot{E}_{D,DORC}$(kW)	38.06
$\dot{E}_{D,PEM}$(kW)	8
$\dot{m}_{H_2}$(kg/h)	0.31

Figures

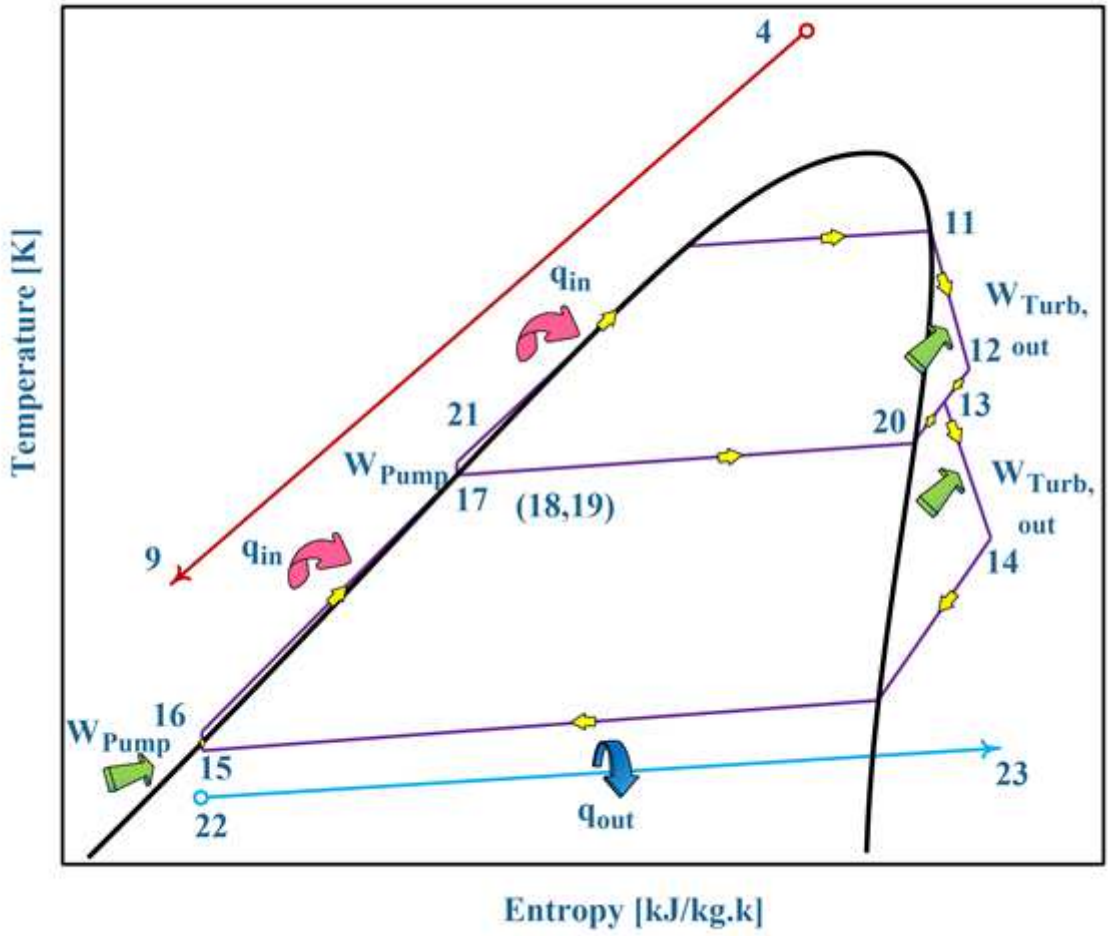

Figure 1

Schematic diagram of proposed combined system.

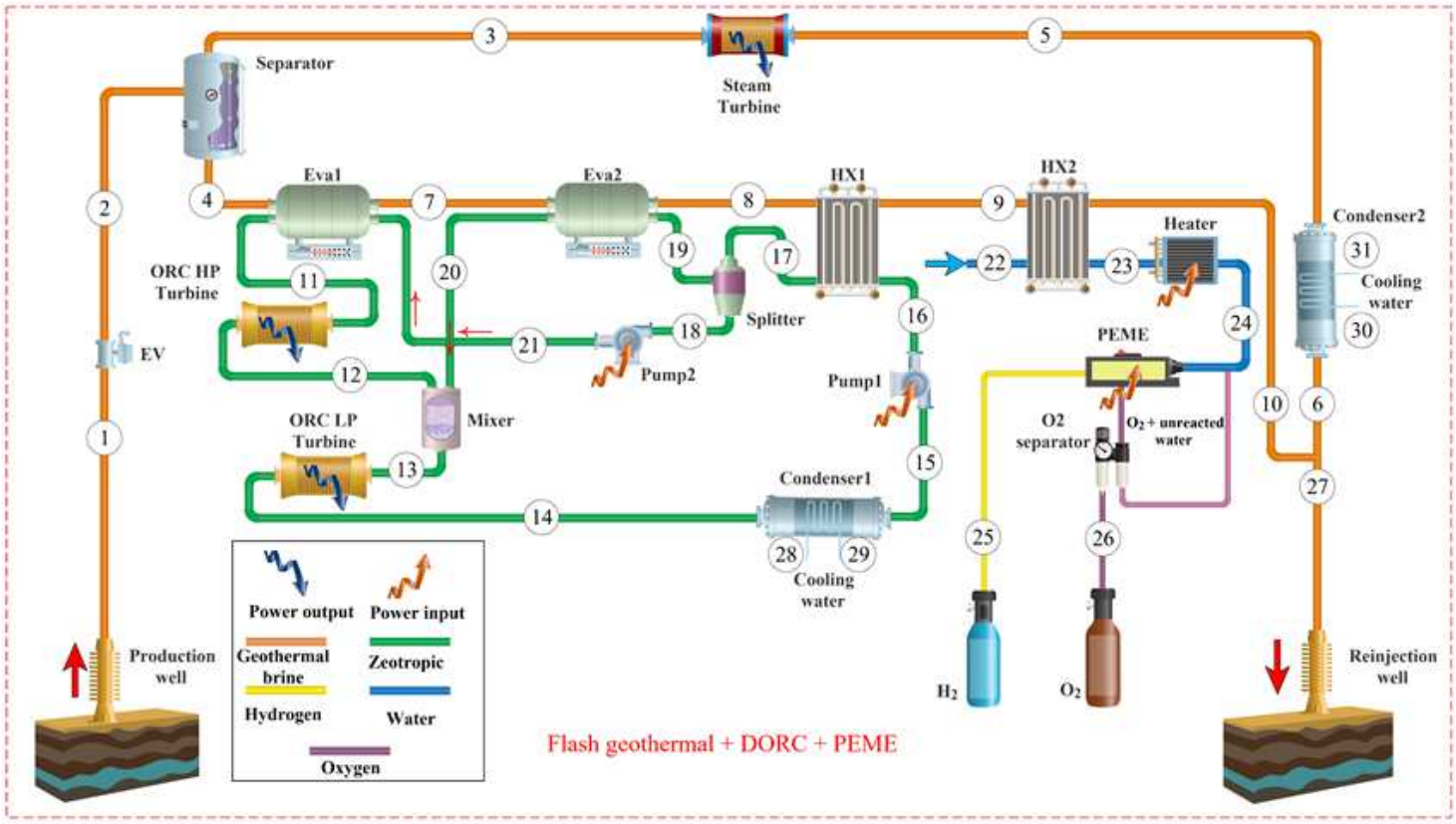

Figure 2

T-s diagram for the dual-pressure organic Rankine cycle

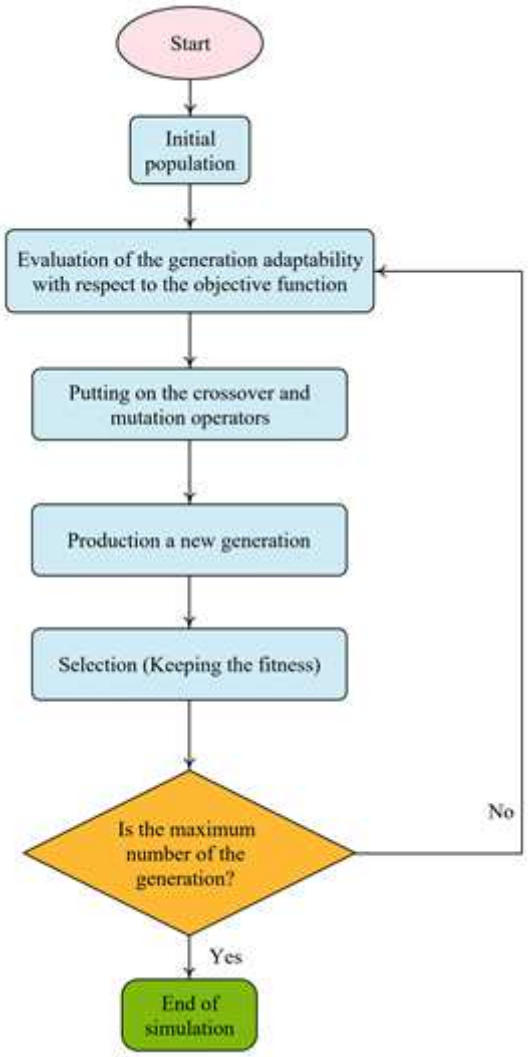

Figure 3

Flowchart of Genetic algorithm.

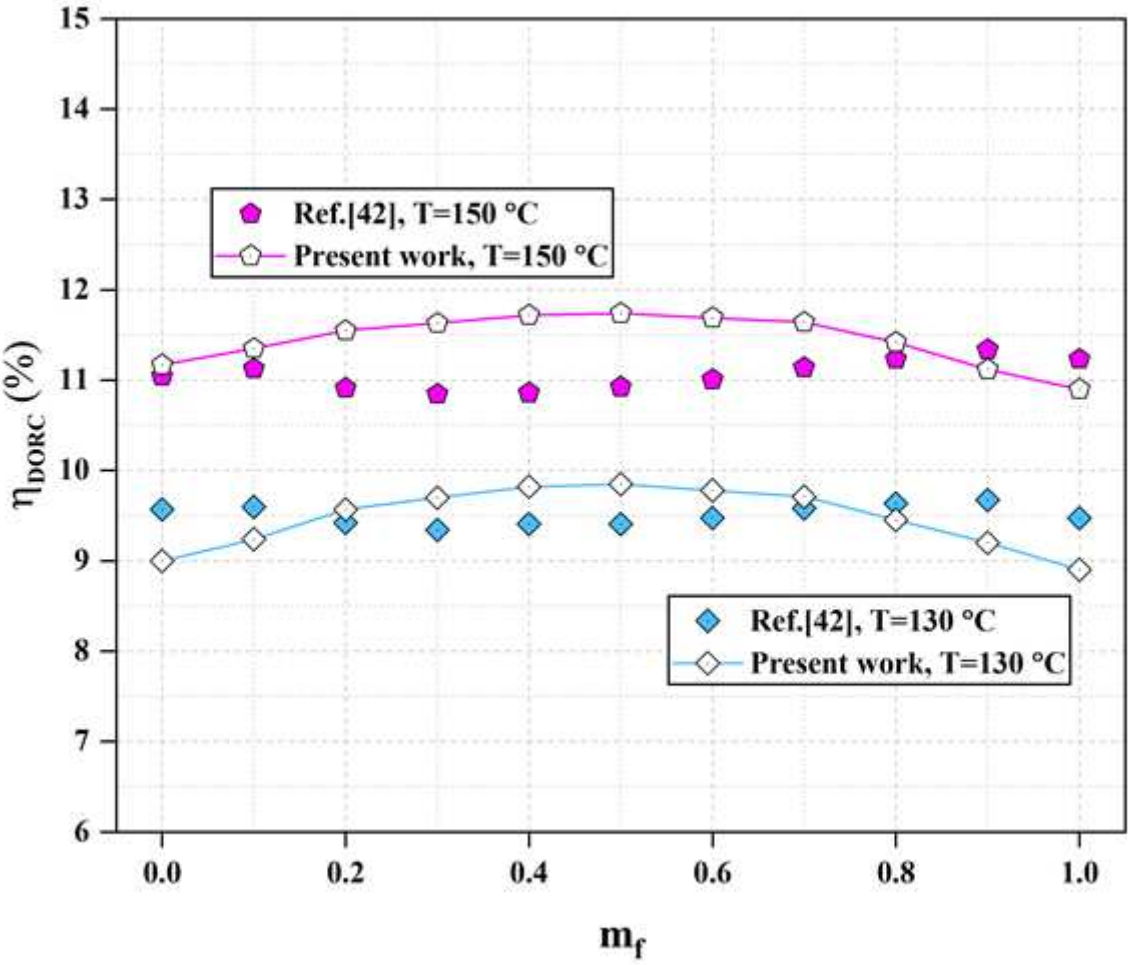

Figure 4

Comparison of the present simulation results with the Li et al.[42] obtained data for DORC unit.

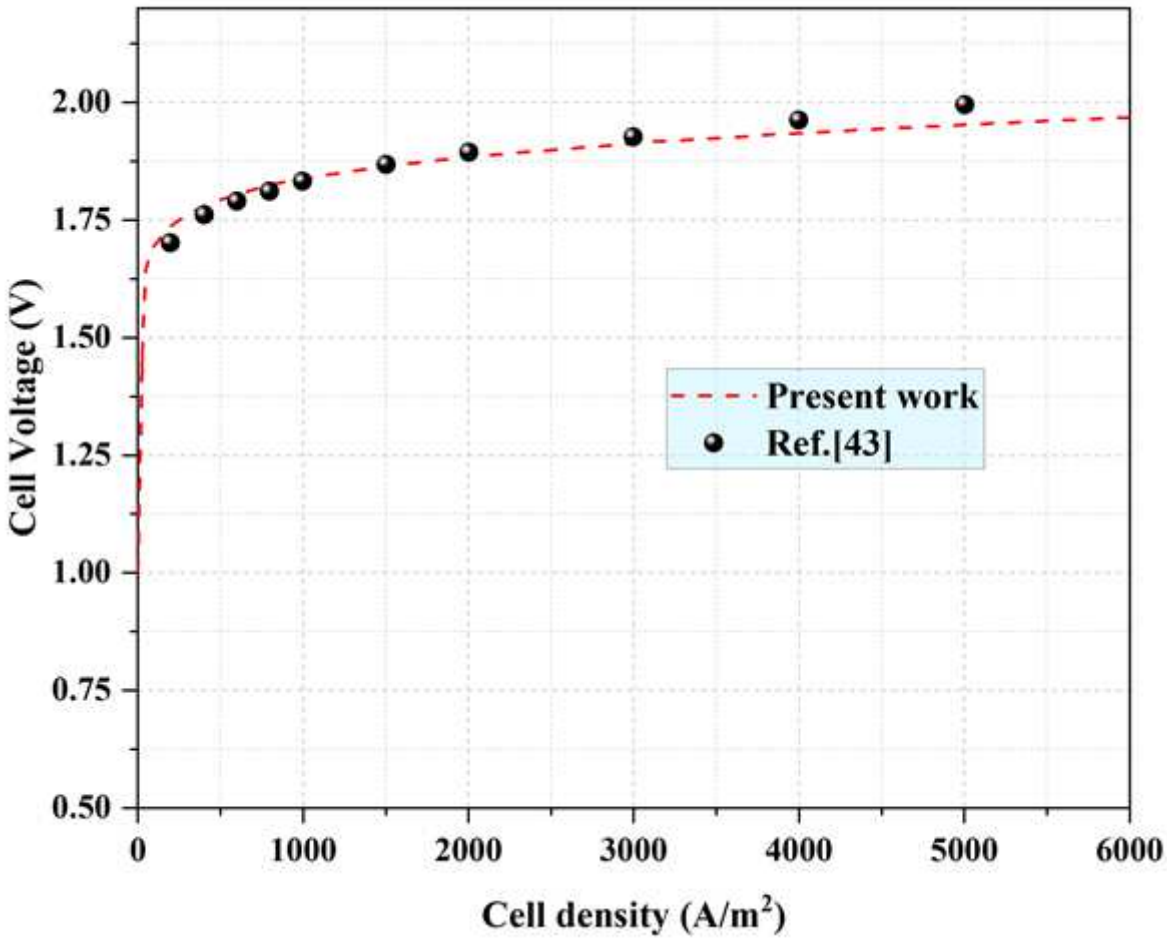

Figure 5

Comparison of the present simulation results with Ref.[43] obtained data for PEM electrolyzer system.

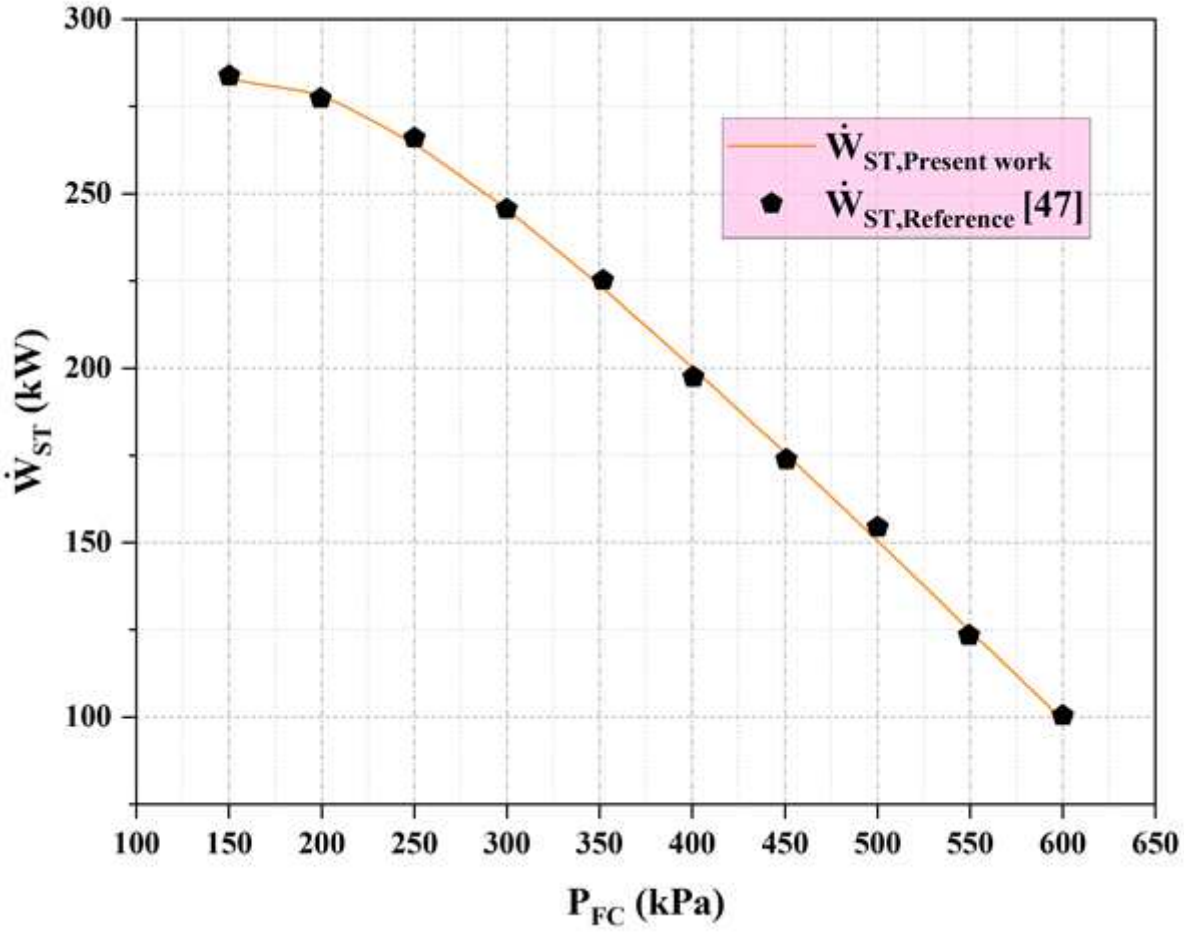

Figure 6

Comparison of the present simulation results with Ref.[41] obtained data for geothermal flash cycle system .

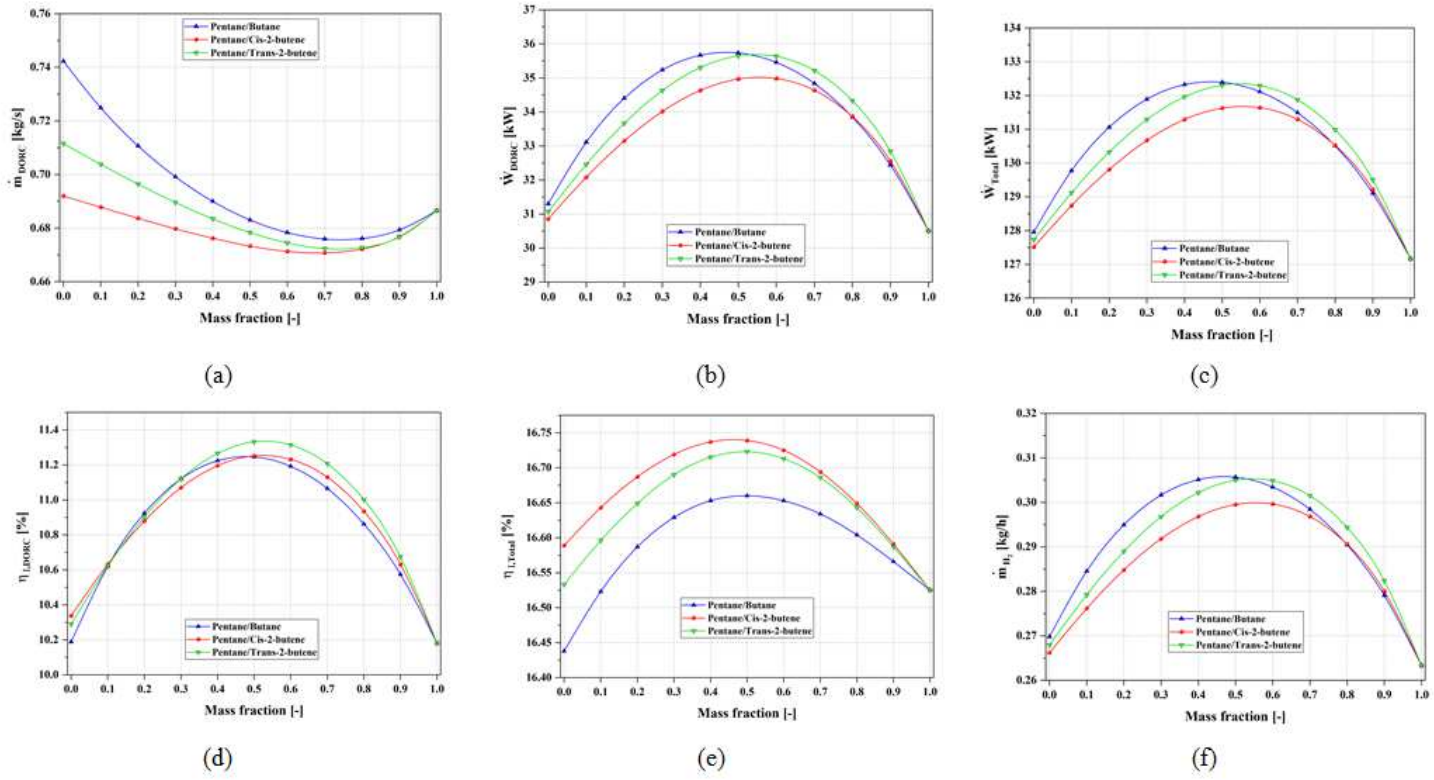

Figure 7

Effect of mass fraction (m_f) on (a) mass flow rate of DORC unit, (b) output work of DORC unit, (c) total net output work, (d) energy efficiency of DRC unit, (e) energy efficiency of entire system, (f) the rate of hydrogen production.

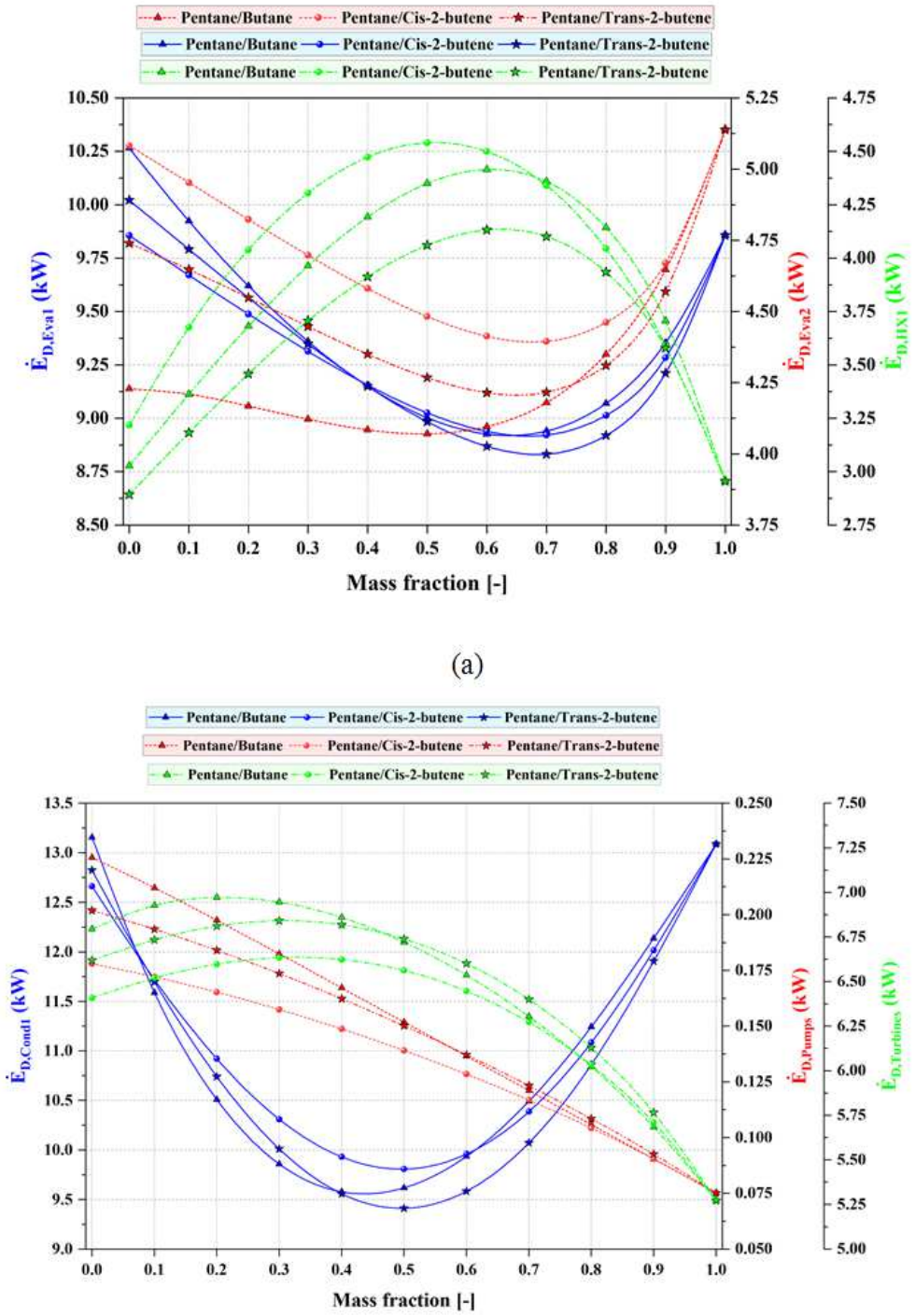

Figure 8

Effect of mass fraction (m_f) on the exergy destruction rate of each components of proposed system.

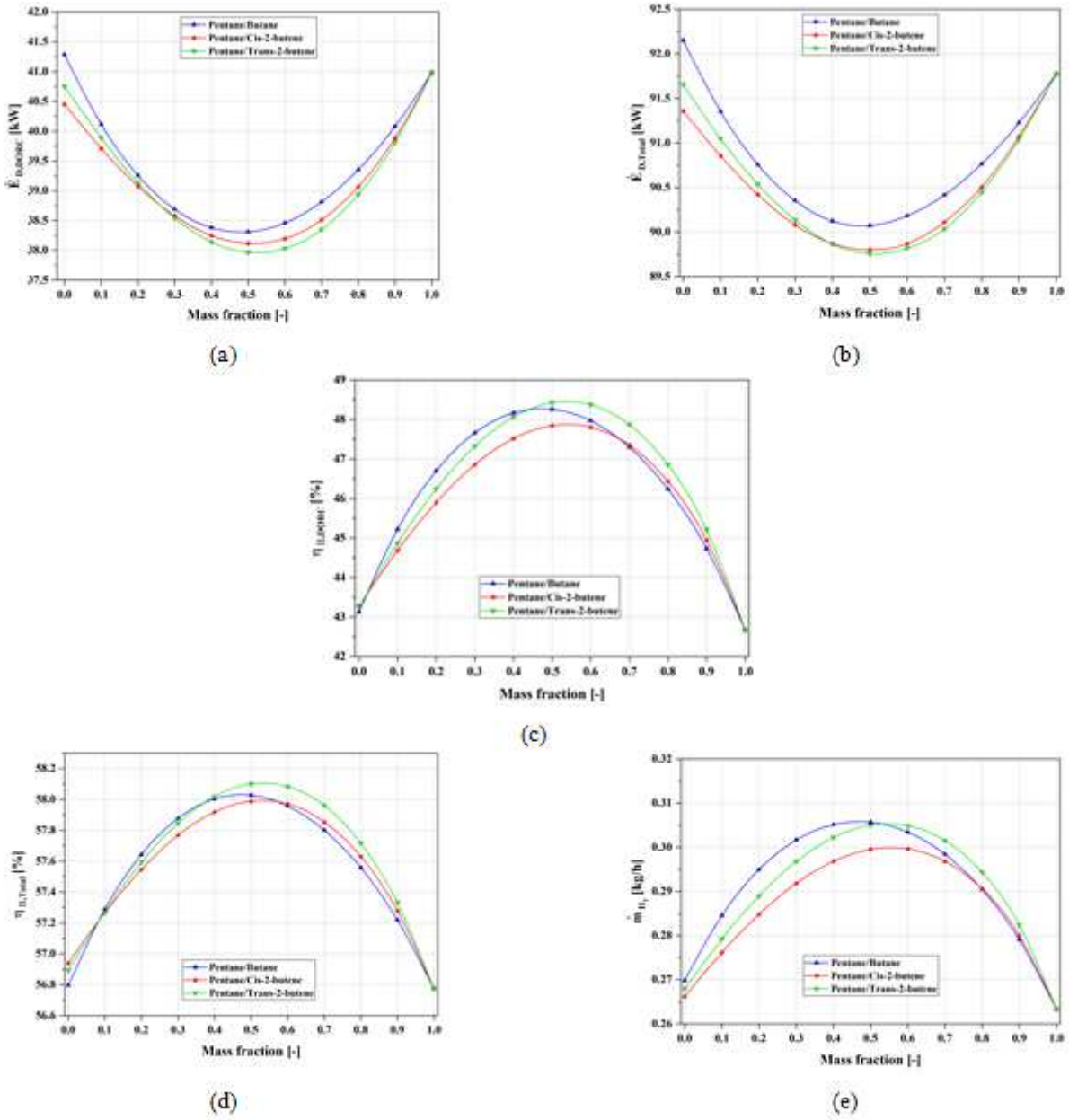

Figure 9

Effect of mass fraction (m_f) on the rate of exergy destruction and exergy efficiency of DORC unit and entire system.

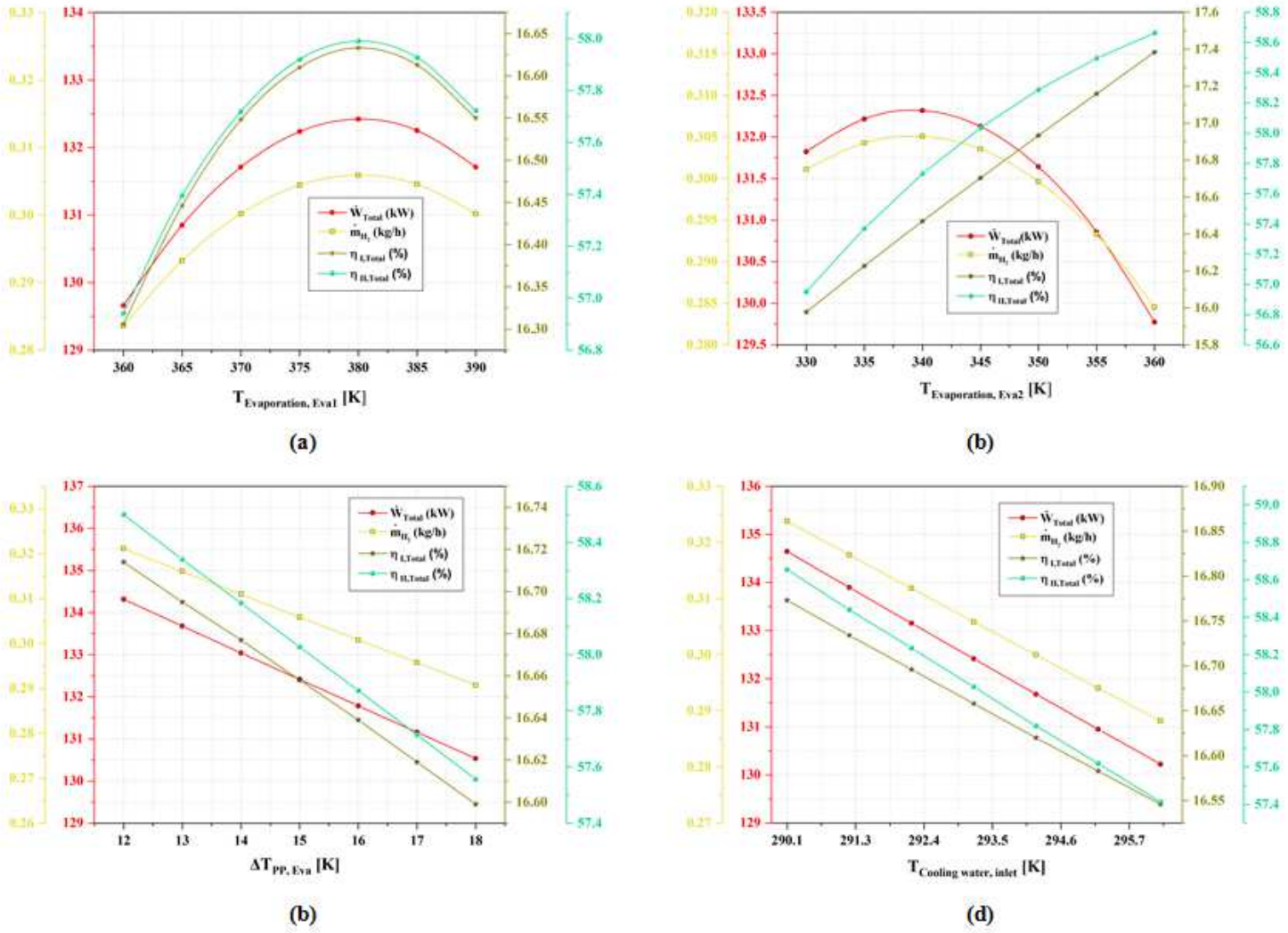

Figure 10

The trend of variation for different performance parameters with T_evaporation (1) and (2), ΔT pp, eva and inlet temperature of cooling water for various working fluids.

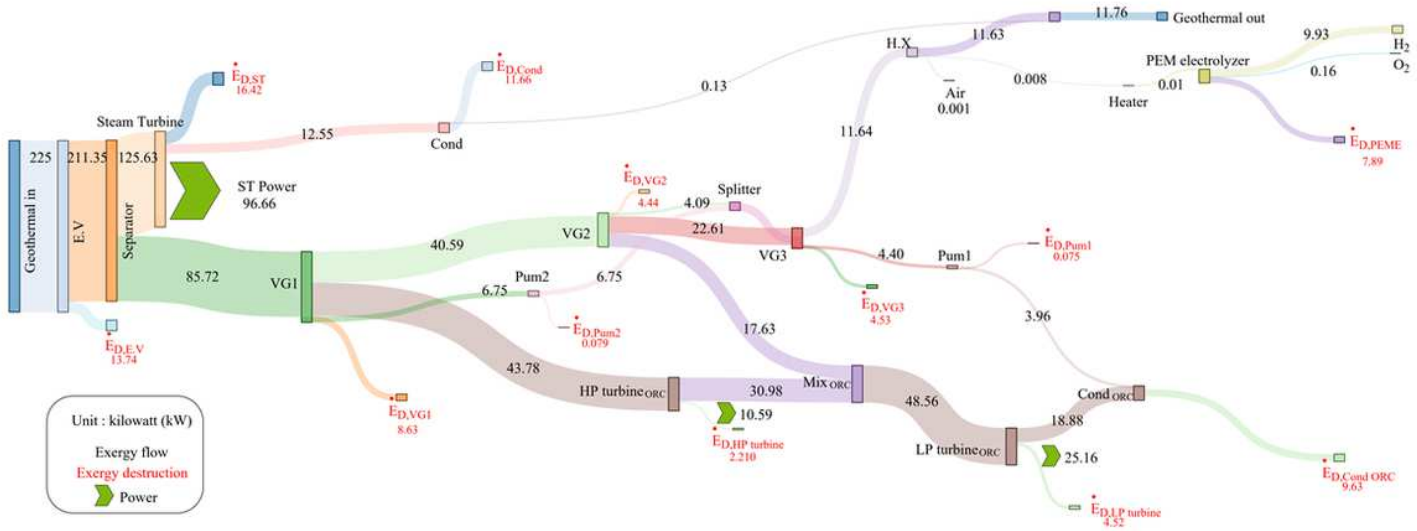

Figure 11

The Sankey diagram of proposed flash-binary geothermal system